

Alma Mater Studiorum Università di Bologna
Archivio istituzionale della ricerca

Atmospheric corrosion of Cu-Si-Mn bronze for contemporary art under simulated runoff and continuous immersion conditions

This is the final peer-reviewed author's accepted manuscript (postprint) of the following publication:

Published Version:

Chiavari, C., Martini, C., Balbo, A., Monticelli, C., Velino, C., Masi, G., et al. (2022). Atmospheric corrosion of Cu-Si-Mn bronze for contemporary art under simulated runoff and continuous immersion conditions. CORROSION SCIENCE, 205, 1-15 [10.1016/j.corsci.2022.110442].

Availability:

This version is available at: <https://hdl.handle.net/11585/889855> since: 2022-09-19

Published:

DOI: <http://doi.org/10.1016/j.corsci.2022.110442>

Terms of use:

Some rights reserved. The terms and conditions for the reuse of this version of the manuscript are specified in the publishing policy. For all terms of use and more information see the publisher's website.

This item was downloaded from IRIS Università di Bologna (<https://cris.unibo.it/>).
When citing, please refer to the published version.

(Article begins on next page)

This is the final peer-reviewed accepted manuscript of:

Cristina Chiavari, Carla Martini, Andrea Balbo, Cecilia Monticelli, Cecilia Velino, Giulia Masi, Elena Bernardi, *Atmospheric corrosion of Cu-Si-Mn bronze for contemporary art under simulated runoff and continuous immersion conditions*, Corrosion Science, 205 (2022) 110442

The final published version is available online at:

<https://doi.org/10.1016/j.corsci.2022.110442>

Rights / License: CC-BY-NC-ND 4.0 license

(<http://creativecommons.org/licenses/by-nc-nd/4.0/>)

The terms and conditions for the reuse of this version of the manuscript are specified in the publishing policy. For all terms of use and more information see the publisher's website.

This item was downloaded from IRIS Università di Bologna (<https://cris.unibo.it/>)

When citing, please refer to the published version.

Atmospheric corrosion of Cu-Si-Mn bronze for contemporary art under simulated runoff and continuous immersion conditions

Cristina Chiavari¹, Carla Martini², Andrea Balbo³, Cecilia Monticelli³, Cecilia Velino⁴, Giulia Masi⁵, Elena Bernardi^{4}*

¹Department for Cultural Heritage, University of Bologna, via degli Ariani 1, Ravenna, Italy, cristina.chiavari@unibo.it

²Department of Industrial Engineering, University of Bologna, viale Risorgimento 4, 40136 Bologna, Italy, carla.martini@unibo.it

³Centro di Studi sulla Corrosione e Metallurgia "A. Daccò", Tecnopolo di Ferrara, Department of Engineering, University of Ferrara, via Saragat 4A, 44122 Ferrara, Italy, andrea.balbo@unife.it

⁴Department of Industrial Chemistry "Toso Montanari", University of Bologna, viale Risorgimento 4, 40136 Bologna, Italy, elena.bernardi@unibo.it, cecilia.velino2@unibo.it

⁵Department of Civil, Chemical, Environmental and Materials Engineering, University of Bologna, via Terracini 28, 40131 Bologna, Italy, giulia.masi5@unibo.it

* Corresponding author: elena.bernardi@unibo.it

Abstract:

Silicon bronze is widely used for monuments: corrosion of Cu-3Si-1Mn was studied with respect to Cu-5Sn-5Zn-5Pb during ageing tests (runoff/full immersion) in acid rain. Surface characterisation (FEG-SEM/EDS elaborated through PCA, TEM, Raman, FTIR, profilometry), metal release and EIS measurements were performed. Under runoff conditions, where mechanical action plays a role, the alloys showed comparable corrosion resistance. In full immersion the corrosion rate of Cu-3Si-1Mn was slightly higher than that of Cu-5Sn-5Zn-5Pb, due to the different nature of the corrosion products. Results showed that, compared to Sn oxide/hydroxide, Si tends to form less protective amorphous products, detaching from the surface.

Keywords: Copper (A); Alloy (A); EIS (B); IR spectroscopy (B); SEM (B); atmospheric corrosion (C)

1. Introduction

The demand of innovative bronze alloys for artistic applications is continuously increasing and attracts research and production interests, while traditional leaded bronze alloys are being progressively abandoned because they contain significant amounts of Pb, which may cause well-known health and environmental issues. Several requirements, such as castability, mechanical, aesthetical properties and corrosion resistance, need to be considered for the development of new Pb-free bronze alloys [1].

Some previous studies investigated the metallurgy, castability and mechanical properties [2] or the corrosion behaviour of innovative tin-bronzes for artistic applications, with respect to traditional ones [1,3,4]. In these works, the addition of Si and/or Ni to Sn-bronzes was considered to reduce the Pb amount. In fact, Si and Ni enhance casting and mechanical properties as well as corrosion resistance [1,2]. Tests carried out in climatic chambers, salt spray cabinet or through continuous immersions showed that the addition of about 3 wt% Si to Cu-(8-10)Sn alloys improves corrosion resistance with respect to Cu-Sn-Zn-Pb bronzes, both in simulated marine and urban environment [3,4], and also with respect to Cu-Sn-Zn ones in simulated urban rain [4]. The better performances of Si-containing bronzes in these conditions were ascribed to the formation of a more compact and stable patina layer. In [1], the authors compared the corrosion behaviour of a Cu-5Sn-5Zn-5Pb bronze with that of Sn-bronzes containing different Si and/or Ni amounts. In this case, salt spray and climate chamber tests showed no improvement or even worst results in term of thickness loss when about 3 wt% Si is added, while the highest improvement was observed by adding Si and Ni, both at 0.8 wt%.

As highlighted, the mentioned studies investigated atmospheric corrosion of innovative bronzes containing Sn, and in conditions simulating sheltered or stagnant exposure, without considering rain runoff. The key role of Sn in bronze corrosion is described in several studies, demonstrating that traditional bronzes behave differently from pure Cu, due to the role of the alloying elements, especially Sn [5–8]. Moreover, sheltered and unsheltered exposure geometries strongly influence the morphological and compositional properties of patinas [9–14]. Specifically, for outdoor bronzes exposed to rain events, if the surface experiences rain stagnation, then the patina acts as a multi-layer system with the precipitation of Cu- and Pb-based compounds [10–12]. Conversely, under runoff conditions, the patina consists of a thin and porous layer strongly enriched in non-soluble Sn oxides and hydroxides, across which Cu, Zn and Pb ions can migrate and be leached in the environment [9,11–14].

Nowadays, artistic foundries widely use cast Pb-free silicon bronzes, that do not contain tin. In particular, Cu-3Si-1Mn bronze (UNS C87300) is usually employed as a substitute for tin-bronze when good physical and corrosion resistance are required [15]. The 1 wt% Mn addition contributes to improve tensile strength and hardness of the Cu-3Si alloy, due to a refinement and modification of the cored dendritic grains; a further increase in Mn to 1.5 wt% causes a slight decrease in both these mechanical properties [16]. Cu-3Si-1Mn alloy is especially employed for bearings, bells, impellers, pump and valve components, marine fittings, as well as statuary and art castings [15]. In the artistic field, beside the good castability, mechanical properties and corrosion resistance, as well as the golden colour, are appreciated.

However, very few studies are present in literature investigating the corrosion behaviour of Si-bronzes, containing significant amounts of Zn (>2 wt%) and lower amounts of Mn (<0.2 wt%) than Cu-3Si-1Mn bronze [17–19]. Moreover, these studies are carried out only under full immersion in soft, hard, drinking water or 3.5 wt% NaCl solution, focusing on technological/industrial applications. In particular, a UNS C87600 drinking water pump impeller was found to suffer from dealloying corrosion via desiliconification of a Si-rich phase; its early failure was attributed to an unknown corrosive agent injected into the stream [18]. A previous study

[20] reported the assessment of the protectiveness of silane-based coatings applied on K₂S-patinated Cu-3Si-1Mn alloy, but it focused on the characterisation of the artificial patina (i.e., the actual substrate for coating application) and on the study of the coating-patina interactions, not on the corrosion behaviour of the bulk alloy.

Given the increasing importance of this alloy in the artistic field and the overall lack of information on its atmospheric corrosion behaviour, the present work focuses on the corrosion mechanism of Cu-3Si-1Mn alloy in simulated outdoor conditions.

Both runoff and continuous immersion exposure conditions were investigated. Runoff test is designed to reproduce the atmospheric exposure of bronze unsheltered areas under the combined action of both the rain solution and the mechanical effect of dripping. The results obtained on Cu-3Si-1Mn bronze are compared with the behaviour of a traditional quaternary leaded bronze used for artistic casting (Cu-5Sn-5Zn-5Pb) already studied in [9,11]. Continuous immersion tests, simulating conditions closer to long-term water stagnation, were carried out on both Cu-3Si-1Mn and Cu-5Sn-5Zn-5Pb bronze to further investigate the main factors affecting the corrosion behaviour of the two alloys. The runoff test (up to a time of wetness of 60 days) was carried out using a dropping test device developed for accelerated ageing bronzes [9]. The bronze microstructure and the surface evolution were characterised by optical microscopy, Scanning Electron Microscopy (SEM) coupled with Energy Dispersive Spectroscopy (EDS), Raman spectroscopy, Fourier Transform Infrared Spectroscopy (FTIR), colour measurements, profilometry, mass variation and mass loss measurements. The corrosion products formed on Cu-3Si-1Mn bronze were also analysed by Transmission Electron Microscopy (TEM) coupled with EDS. The weathering solutions were analysed by Atomic Absorption Spectroscopy (AAS) in terms of Cu, Si and Mn soluble species concentrations, to attain a deeper knowledge of the corrosion process. Electrochemical impedance spectroscopy (EIS) and SEM/EDS were used to monitor the evolution of the corrosion process during full immersion tests, where only the chemical effect of rain solution is active.

2. Material and methods

2.1 Bronze specimens

The composition of bronze, supplied by Livartis Foundry d.o.o, Slovenia, corresponds to UNS C87300 [15,21] and contains 3.1±0.4 Si and 0.9±0.1 Mn (wt%) as main alloying elements. Sn and Zn (< 0.1 wt%) as well as P (0.02 wt%) are also present as trace elements (GDOES data from the supplier). As-cast plates (5 mm thick) were obtained by sand casting.

For metallographic investigations and accelerated ageing tests in runoff condition, the Cu-3Si-1Mn bronze plate was cut to obtain 50 mm x 25 mm samples that were SiC-polished (P1000 grade) before exposure. Microstructural characterisation of the alloy was carried out by Reflected Light Optical Microscopy (RLOM, Zeiss AXIO Imager A1m) and scanning electron microscopy (SEM, Zeiss EP EVO 50) with energy dispersive X-ray spectroscopy (EDS, Oxford Instruments INCA ENERGY 350). Before observation, chemical etching (by FeCl₃/HCl in ethanol) was used for highlighting specific microstructural features.

For full immersion tests, square specimens with an exposed surface area of 1 cm² were soldered to sheathed copper wires to ensure electrical connection and were then embedded in epoxy. Before immersion in the aggressive solutions, the electrode surface was prepared by SiC emery paper up to P-1000 grade and were then polished with 1 µm diamond powder to a mirror finishing. Finally, they were washed with deionized water and degreased with ethyl alcohol. Some tests were performed on cast Cu-5Sn-5Zn-5Pb plates used as

benchmark. The Cu-5Sn-5Zn-5Pb is a quaternary bronze with dendritic microstructure of cored α solid solution where Sn segregation occur at dendrite border. Sn-rich precipitates and Pb globules are observed in the interdendritic areas [5]. The Cu-5Sn-5Zn-5Pb bronze composition is reported in Table S3 in the supplementary material section.

2.2 Aggressive solution

The test solution consisted of an artificial rain (AR) with pH 4.35, prepared according to the composition of the natural acidic rain collected in Bologna (Italy) and synthesized according to the recipe reported in [23]. The ion concentrations were: SO_4^{2-} 1.90 mg L⁻¹, Cl^- 1.27 mg L⁻¹, NO_3^- 4.62 mg L⁻¹, CH_3COO^- 0.23 mg L⁻¹, HCOO^- 0.05 mg L⁻¹, NH_4^+ 1.05 mg L⁻¹, Ca^{2+} 0.34 mg L⁻¹, Na^+ 0.53 mg L⁻¹.

2.3 Runoff accelerated ageing

Cu-3Si-1Mn bronze samples were aged by using a dropping device and applying the experimental conditions reported in previous studies on atmospheric corrosion of Cu-5Sn-5Zn-5Pb quaternary bronzes [9,11], so as to compare the results. In particular, the AR solution was guttered in single drops on the bronze samples inclined by 45°, with a dropping rate of 60 mL/h and a drop fall height of 4 cm. The solution was periodically dropped on the bronze samples following a weekly cycle of 3 days dropping/1day dry/2 days dropping/1 day dry, up to a total time of wetness (ToW) of 60 days. During the test, both the evolution of the corrosion attack morphology and the metal release in AR (details in section 2.3.1 and 2.3.2, respectively) were monitored, together with thickness and mass variations. In addition, polished cross-sections were prepared and analysed. Corrosion rate was also determined.

2.3.1 Characterisation of bronze specimens

Optical microscope and Scanning Electron Microscope (SEM) observations associated to Energy Dispersion Spectroscopy (EDS) analyses (ZEISS EVO MA 15 SEM model, equipped by an Aztec Oxford apparatus for EDS analysis, SDD detector) were performed to investigate the alloy microstructure and the evolution of the corrosion morphology during both continuous immersions and accelerated corrosion tests. The SEM characterisation of the alloy microstructure as well as the patina morphology and composition were carried out under an accelerating voltage of 20 kV and 10 kV, respectively. EDS analyses were carried out both on large areas (1.0 x 0.5 mm²) and single spots.

To better explore the similarities among surface spot analyses collected during accelerated ageing, EDS data were elaborated through the chemometric technique Principal Component Analysis (PCA). This multivariate statistical tool allows to reduce the dimensionality of a dataset by retaining only the relevant information. An orthogonal linear transformation is applied to the original variables to obtain a new coordinate system formed by uncorrelated variables (Principal Components, PC) perpendicular to each other. The first PC is oriented in the direction representing the maximum variability in the data; each of the subsequent PCs describes the maximum of the remaining variability [22,23]. PCA results can be visualised as scatter plots of *scores* and *loadings*, representing respectively the projections of the original objects (e.g., localised EDS analyses) and variables (e.g., analysed metals) in the new PCs space. A dataset consisting of 196 objects (the different EDS localised analyses) and 3 variables (Cu, Mn and Si) was analysed through the R-based freeware CAT (Chemometric Agile Tool). Data were subjected to centring and scaling pre-treatments to make all variables comparable. According to the Score Test, two principal components were chosen, giving an explained variance of 97.9%.

Phase composition of the corroded surfaces was analysed by Raman analysis with a Renishaw Raman Invia Spectrometer configured with a Leica DMLM microscope and an Ar⁺ laser (514.5 nm) as excitation source. The corrosion products produced during accelerated ageing were collected by mild surface grinding with KBr powder and then analysed by Fourier Transform Infrared (FTIR) spectroscopy using the DRIFT (Diffuse Reflectance Infrared Fourier Transform) accessory mounted on a Thermo-Scientific Nicolet iS50 spectrometer (Thermo Fisher Scientific, Waltham, USA). During the analyses, the spectrometer was purged with dry, CO₂-free air generated with a Balston 75–52 unit and a deuterated triglycine sulphate (DTGS) detector permitted to investigate the region from 4000 to 400 cm⁻¹, with a resolution of 4 cm⁻¹.

In addition to these spectra, high-resolution transmission electron microscopy (TEM) observations were performed by a TEM STEM FEI TECNAI F20 microscope also coupled with EDS. The applied accelerating voltage was 200 keV. The corrosion products in correspondence of the dendrite borders, periodically collected on a glass plate with a thin needle during ageing of a sample specifically used for this purpose, were directly deposited on a holey C-film supported by an Au grid.

During the AR dropping test (at ToW values of 15, 30 and 60 days), the colour of the aged bronze surfaces was measured in the CIELab colour space using a Datacolor D400 spectrophotometer operating with d/8° geometry, D65 illuminant, 10° observer, 6.6 mm aperture and specular component excluded (SCE). CIELab space defines three coordinates for each colour: L* corresponding to Lightness (ranging from 0 (black) to 100 (white)), a* and b* corresponding to the chromatic coordinates (+a* is red, -a* green, +b* is yellow, -b* blue). The colour of each sample was determined by averaging three measurements recorded on the aged area. The total colour variation (ΔE^*) with respect to the unexposed surface was calculated using the following equation, $\Delta E^* = (\Delta L^{*2} + \Delta a^{*2} + \Delta b^{*2})^{1/2}$.

Gravimetric measurements were carried out on dry days during ageing, by a digital balance KERN AGB210_4 with sensitivity of ± 0.1 mg. The mass variation (in μg) was divided by the area of the sample actually wetted by the AR droplets (in cm^2). In addition, roughness profiles were recorded at different exposure times by a stylus profilometer (tip radius of 5 μm , precision 0.2 μm) to measure the progressive thickness variation induced on the bronze surface by the corrosion process as a function of the exposure time.

At 30 and 60 days of ToW, the sample mass losses were also evaluated after surface cleaning from corrosion products by a deaerated 20 wt% HCl solution [24]. The cleaning procedure consisted in a preliminary washing in distilled water (3.3 ml cm^{-2}) for 30 s, followed by an immersion step in deaerated 20 wt% HCl (5.3 ml cm^{-2}) for 1 min and washing in distilled water for 30 s. All steps were carried out in ultrasonic bath, at room temperature. In order to exclude the contribution of the base metal dissolution during the cleaning procedure, the same cleaning test was replicated on reference samples not exposed to dropping test. After pickling, roughness profiles were recorded to calculate the average thickness loss induced by the corrosion process. Finally, the corrosion rate, v_{cor} (in $\mu\text{m}/\text{day}_{\text{ToW}}$), was determined from thickness loss, as in [9,11].

2.3.2 Characterisation of the artificial rain solution during the ageing

The AR solution dropped on the bronze surface during each dropping phase was separately collected in canisters, then sampled in HDPE bottle, acidified with HNO₃ 65% Suprapur and stored at 4°C to analyse the metallic ion release. The concentration of alloying elements (Cu, Si, Mn) dissolved in the AR solutions was analysed by Microwave Plasma-Atomic Emission Spectrometer (MP-AES, Agilent 4210), reaching a Limit of Detection of 1 $\mu\text{g}/\text{L}$ for Cu, 0.3 $\mu\text{g}/\text{L}$ for Mn and 10 $\mu\text{g}/\text{L}$ for Si.

2.4 Full immersion ageing and electrochemical tests

Cu-3Si-1Mn and Cu-5Sn-5Zn-5Pb bronze specimens were fully immersed in unstirred AR solution for 15 days. The evolution of the corrosion process was monitored by electrochemical impedance spectroscopy (EIS). A PAR/ AMETEK PARSTAT2273 potentiostat/galvanostat was used by applying the following experimental conditions: ± 10 mV rms alternating potential signal with respect to the corrosion potential (E_{cor}), 10 kHz – 1 mHz frequency range (10 kHz – 10 mHz for immersion times shorter than 1 day) and 5 frequencies/decade. The spectra were fitted by SAI ZView v.3.5c software, according to the most suitable equivalent circuit, as described in the text. The tests were performed in triplicate. All the potentials quoted in the text are related to the Saturated Calomel Electrode (SCE) reference electrode.

The corroded surfaces were periodically analysed also by SEM-EDS.

3. Results and Discussion

Microstructural characterisation of the as-cast Cu-3Si-1Mn bronze will be firstly described and discussed. Subsequently, the effects of accelerated ageing under AR runoff condition (detected by surface and cross-section examination of corroded bronze, as well as by analyses of the leaching solutions at different exposure times) will be reported, followed by the results of electrochemical tests in full immersion condition.

3.1 Microstructural characterisation of as-cast Cu-3Si-1Mn

The metallographic examination of the alloy (Figure S1 in the supplementary material section) revealed a typical dendritic structure with shrinkage cavities in interdendritic spaces (Figure S1a). In addition, marked micro-segregation (i.e., coring) was observed (Figure S1b), leading to Si and Mn enrichment at dendrite borders, where a heterogeneous microstructural constituent was detected (Figures S1c and d). It was characterised by a lamellar morphology (Figure S1d) and was ascribed to an eutectic phase transformation, as discussed in [25].

SEM micrographs reported in Figure 1 confirmed the presence of shrinkage cavities as well as heterogeneous microstructural constituents in the interdendritic spaces. In particular, Figures 1c and d clearly show the lamellar morphology of the eutectic microconstituent. Moreover, the presence of non-metallic inclusions within the eutectic microconstituent was assessed (Figure 1d).

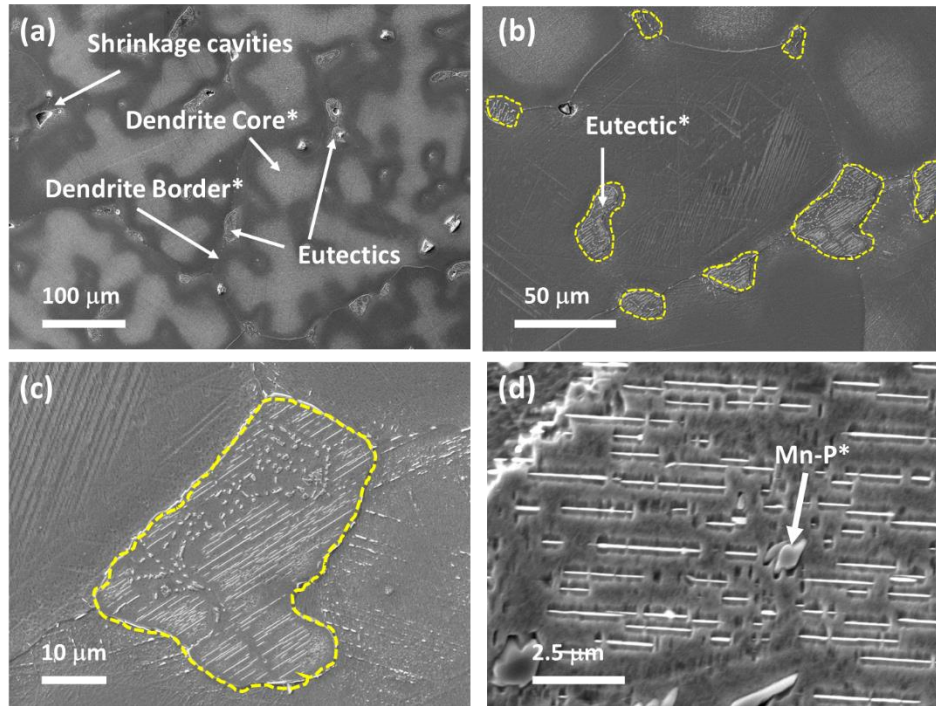


Figure 1: SEM micrographs of the Cu-3Si-1Mn microstructure, highlighting shrinkage cavities and heterogeneous microstructural constituents (evidenced by yellow dotted lines in (b) and in (c)). Stars indicate areas of analysis reported in Table 1.

The EDS elemental analyses reported in Table 1 detected Si and Mn segregation in the interdendritic spaces (i.e., dendrite borders), with concentrations of these elements higher than in the alloy (“General” in Table 1) and in the dendrite core. Even higher Si and Mn concentrations were found in the interdendritic eutectic microconstituent, formed by alternating lamellas of α -Cu solid solution and Cu-Si-Mn phase. Finally, the non-metallic precipitates within the eutectic mostly consisted of Mn and P (hence presumably Mn phosphides, since Mn is known to act as a phosphide- and sulphide-forming element, improving fatigue resistance of bronzes [26]).

Table 1: Elemental analysis (wt%) by EDS of the alloy, considering the different morphologies observed in SEM micrographs of Figure 1 (areas of analysis are indicated by stars). Standard deviation of the general alloy composition is also reported.

Areas of analysis	Si	P	Mn	Fe	Cu
General	3.5±0.2	-	0.8±0.2	0.1±0.1	95.6±0.5
Dendrite core	2.8	-	0.7	-	96.5
Dendrite border	3.9	-	1.7	-	94.4
Eutectic	5.7	0.2	3.9	-	90.2
Mn-P precipitate	4.2	12.8	46.2	-	36.8

3.2 Runoff accelerated ageing: surface characterisation

Accelerated ageing tests simulating unsheltered outdoor conditions were performed through dropping tests. The evolution of the surface appearance during accelerated ageing was followed by visual observation and by measuring the colour variation (by comparison to unexposed sample, ToW = 0 day) as a function of ToW (Table 2). Specifically, the initial pale gold yellow surface ($L^*=70\pm2$, $a^*=5.8\pm0.2$, $b^*=14.8\pm0.6$) evolved towards a general orange hue.

Table 2: Colour variation in CIE Lab colour space induced by accelerated ageing on Cu-3Si-1Mn bronze. Values reported correspond to the average of the variations of three different samples and the related standard deviations.

ToW [days]	ΔL^*	Δa^*	Δb^*	ΔE^*
15	-13.3 ± 0.8	-3.6 ± 0.9	10 ± 2	17 ± 2
30	-14.4 ± 0.4	-1.8 ± 0.2	12 ± 2	19 ± 1
60	-11.5 ± 0.6	1.6 ± 0.6	7 ± 1	13.5 ± 0.4

The most significant colour change occurred during the first 15 days of ToW ($\Delta E^*=17\pm2$), then the colour remained quite stable, indicating that the most evident modifications of corrosion products, by comparison to the unexposed surface, occurred in the first period of the exposure.

The evolution of the surface morphology was investigated by optical and SEM observations. As highlighted by colour measurements, the overall surface morphology did not change significantly after 15 days of ToW (optical images in Figure 2). The runoff action of AR highlighted the cored microstructure of the alloy, leading to the formation of craters with gel-like products in interdendritic areas. No other significant morphology variation was observed at this scale.

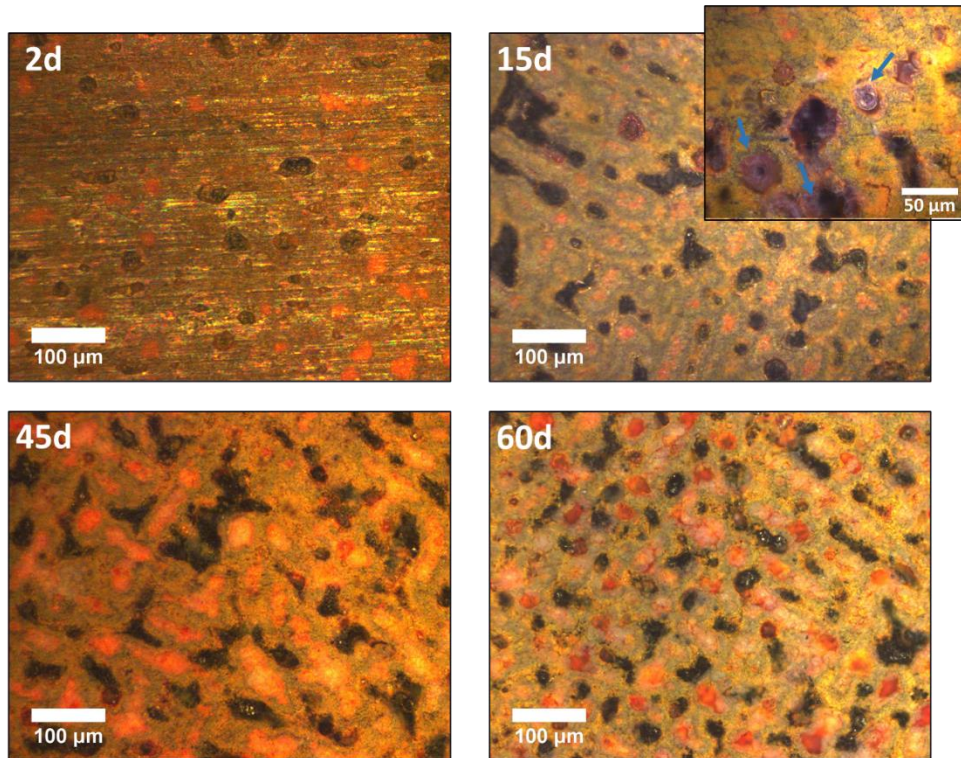
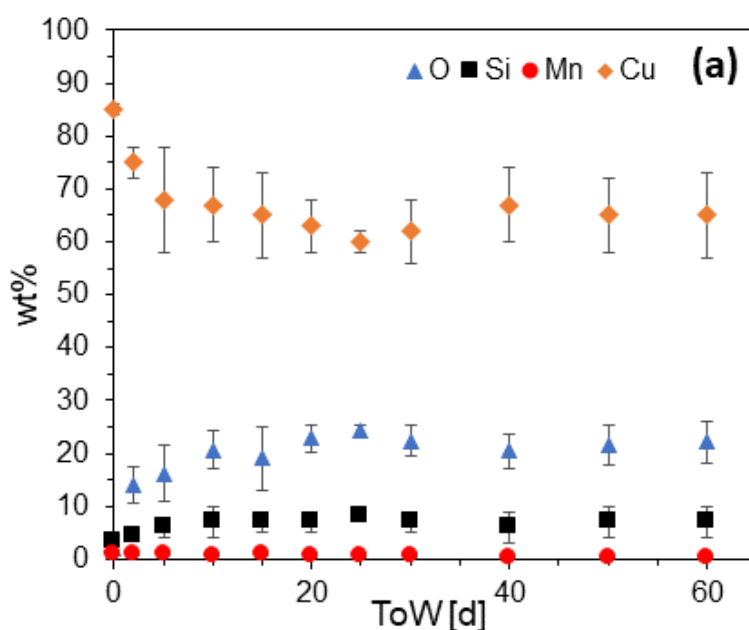


Figure 2: Optical micrographs showing the surface evolution of Cu-3Si-1Mn bronze as a function of exposure time (ToW = 2, 15, 45 and 60 days). A highlight of gel-like products (pointed out by arrows) is reported in the higher magnification picture at 15d of ToW.

The evolution of the overall composition of the corroded surface with exposure time was monitored by EDS analyses on large areas (Figure 3, Table S1). In general, a relative decrease in Cu and Mn species was observed with increasing ToW, in association with a strong Si and particularly O increase, especially up to 25 days of ToW. This can be compared with the behaviour under dropping test of the Cu-5Sn-5Zn-5Pb-bronze, reported in a previous study [9], in which a relative decrease of Cu and Zn in the corroded surfaces indicated the dissolution of these elements and their fairly soluble oxides, inducing a relative Sn enrichment in the patina due to the formation of insoluble corrosion compounds (pK $\text{Sn}(\text{OH})_4$ about 56 and pK SnO_2 about 64 [27,28]). Considering the Cu-3Si-1Mn alloy under investigation, the patina, in runoff conditions, tends to become depleted in Cu and Mn and enriched in Si, even if Si enrichment was lower than that of Sn in quaternary bronzes. With respect to Sn oxide and hydroxide, whose solubility is very low, Si tends to form complex silicates and $\text{Si}(\text{OH})_4$ at pH < 12 [28], however hydrated silica tends to form colloidal compounds which can flocculate and absorb on the surface in the form of a gel. These Si gel-like compounds are less adherent and protective than Sn-products and tend to be removed in runoff condition. However, for prolonged exposure times (ToW > 30 days), Cu/Si and Mn/Si ratios decreased more slowly compared to the first 30 days of ToW, suggesting the achievement of a stationary condition in the second phase of exposure (up to 60 days).



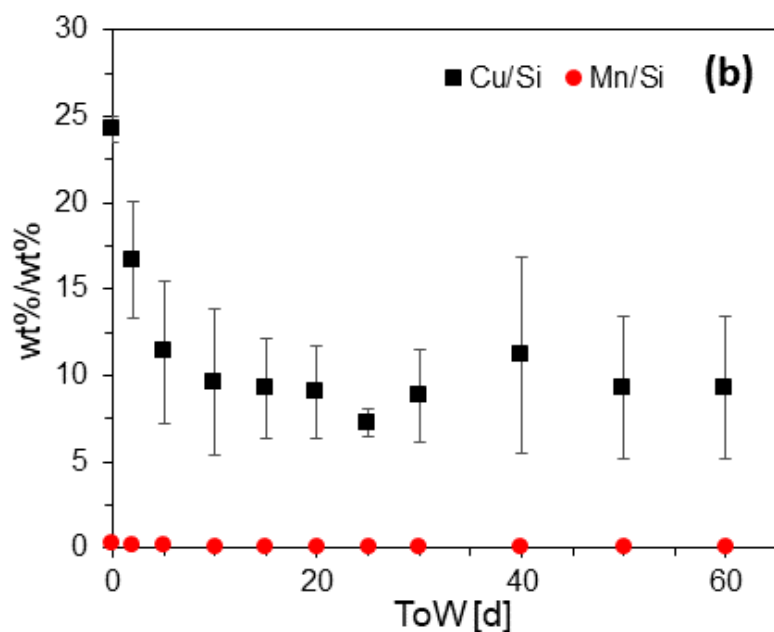


Figure 3: (a) Elemental analysis (wt%) of the corroded surfaces at different time of exposure measured by EDS on large areas (average values and standard deviations). (b) Cu/Si and Mn/Si ratios (wt%/wt%) with related error. Semiquantitative C data are not included in this graph but are available in Table S1 in the supplementary material section.

In order to highlight the behaviour of Mn and Si during ageing, the M/Cu ratios (M= Mn or Si) normalized to the corresponding ratios at ToW = 0 days, $(M/Cu)_{ToW=x}/(M/Cu)_{ToW=0}$, were calculated on the basis of EDS data (Figure 4). Specifically, overall data from large areas were plotted as a function of ToW. As shown in the plot, the Mn ratio tends initially to remain constant, with values close to the ratio in the alloy, and slightly decreases after 20 days of ToW. Conversely, the patina progressively becomes enriched in Si with an oscillating trend: after an initial increase, Si slightly decreased between 25 and 35 days, then increased again and stabilised.

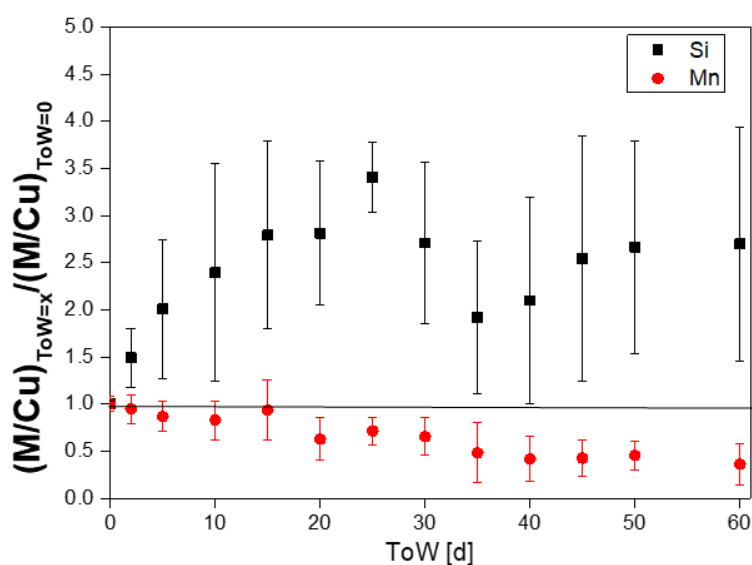


Figure 4: Ratio of M/Cu (M=Si or Mn) as a function of ToW, normalized considering the elemental concentration ratio.

To specifically investigate the corrosion behaviour of the interdendritic microconstituents, localised EDS analyses were performed, at different ToWs, on darker spots (Figure 5, BSE images) and the results were elaborated through PCA.

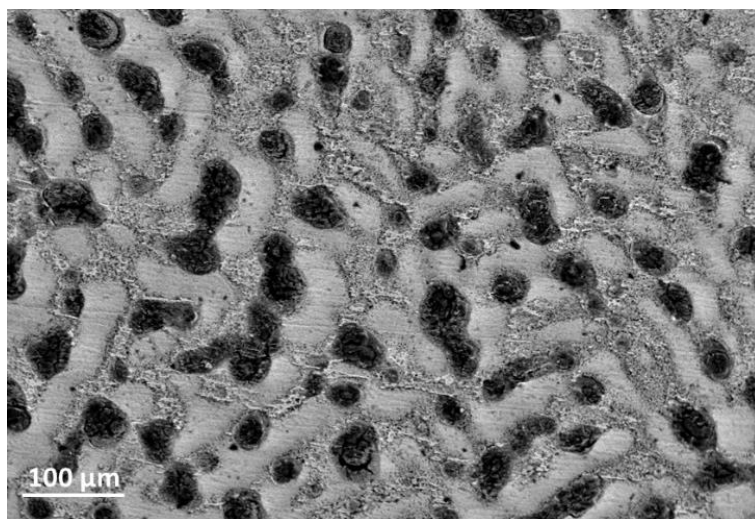


Figure 5: BSE Image of the Cu-3Si-1Mn bronze surface after 5 days of ToW, showing darker spots at dendrite borders.

Figure 6a shows the loadings and scores plot of the first (PC1) and second (PC2) principal components, which explain the 74.3% and the 23.6% of the variance, respectively. The first component (PC1) is mainly related to the amount of Cu (with negative PC1 loading) and Si (with positive PC1 loading) in corrosion products. For each object (darker spot), the more positive the PC1 value, the higher the Si content and the lower the Cu one; the opposite is true for negative PC1 values. Therefore, spots positioned in the first and fourth quadrant of the plot are enriched in Si by comparison to those in the second and third quadrant, whose corrosion products are, on the contrary, characterised by a higher Cu content. The second principal component (PC2) is instead mainly related to the Mn amount (with negative PC2 loading): the more negative the PC2 value, the higher the Mn content in the spot and viceversa. Observing the plot, almost half of the analysed spots appear richer in Si, while the others are richer in Cu. Therefore, in order to evaluate the frequency of the two different types of spots at the different ageing time, the scores values on PC1 were plotted as a function of ToW (Figure 6b). The score value corresponding to the interdendritic eutectic microconstituents before ageing (EDS data in Figure 3, Table S1) is reported at ToW=0 days.

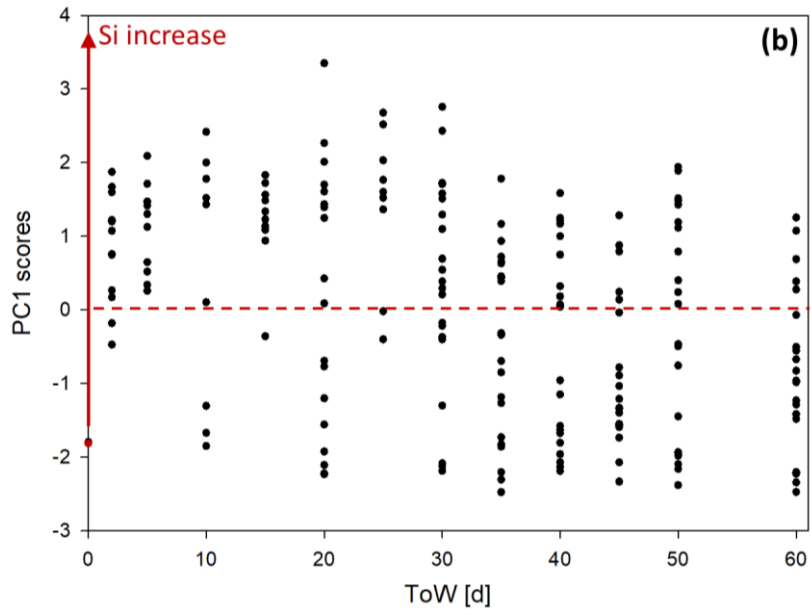
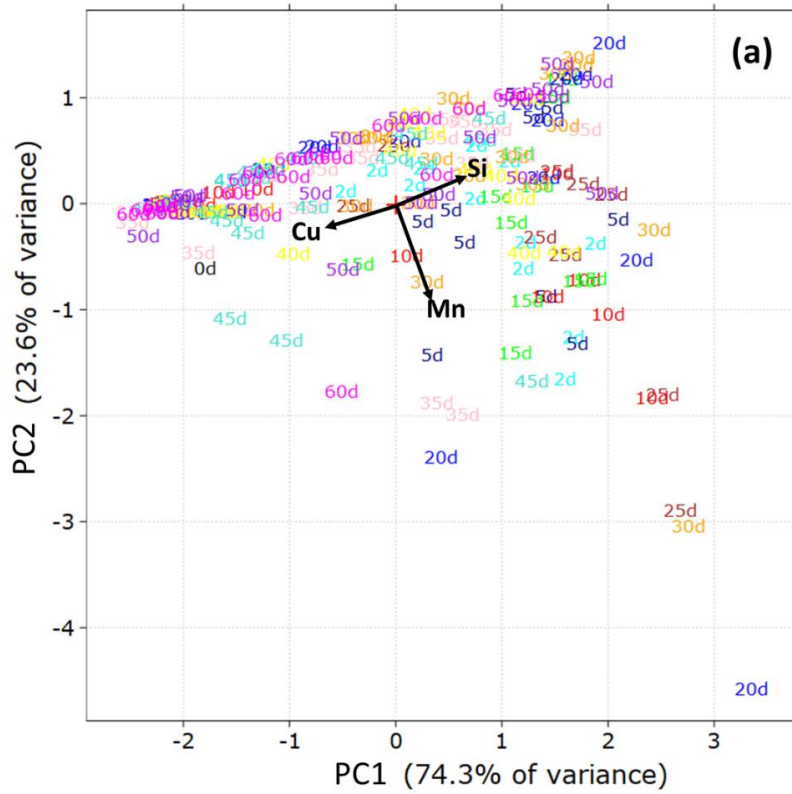


Figure 6: (a) Loading and Score plot for the first (PC1) and the second (PC2) component of the PCA model related to the EDS analyses of dark spots performed at different ToW. PC1 and PC2 explain 74.3% and 23.6% of the total variance, respectively. Variables included in the model are the amounts of Cu, Mn and Si. Objects, corresponding to the spots analysed, are labelled with the related days of ToW. (b) PC1 Scores plotted as a function of ToW of the related objects.

The score plot in Figure 6b shows that at the beginning of the ageing process, all the spots tend to become Si-enriched with increasing exposure time (positive values on PC1), whilst after 10 days two groups start to stand out, one still Si-enriched and the other more similar to the initial composition of the interdendritic

eutectic microconstituents (negative values on PC1). The two groups start to be similarly populated after 30 days of ToW. These data suggest the formation of Si-enriched compounds that, after 10 days of ToW, start to partially detach (as subsequently discussed in section 3.4), attaining a nearly stationary condition after 30 days of ToW. The same elaboration of PC2 scores shows that Mn amount in the spots tend to progressively decrease with time (see Figure S2).

In order to better understand the heterogeneity of the corroded surface highlighted by PCA analysis of EDS data, cross-sections were prepared across the two different groups of interdendritic spots (both Si-enriched and non-enriched ones). Figure 7 shows such spots on the corroded surface after 60 days of ToW, together with EDS data (Figure 7a) and the corresponding cross-sections (Figures 7b, c and d) with X-ray maps of the corrosion craters (Figures 7c and d).

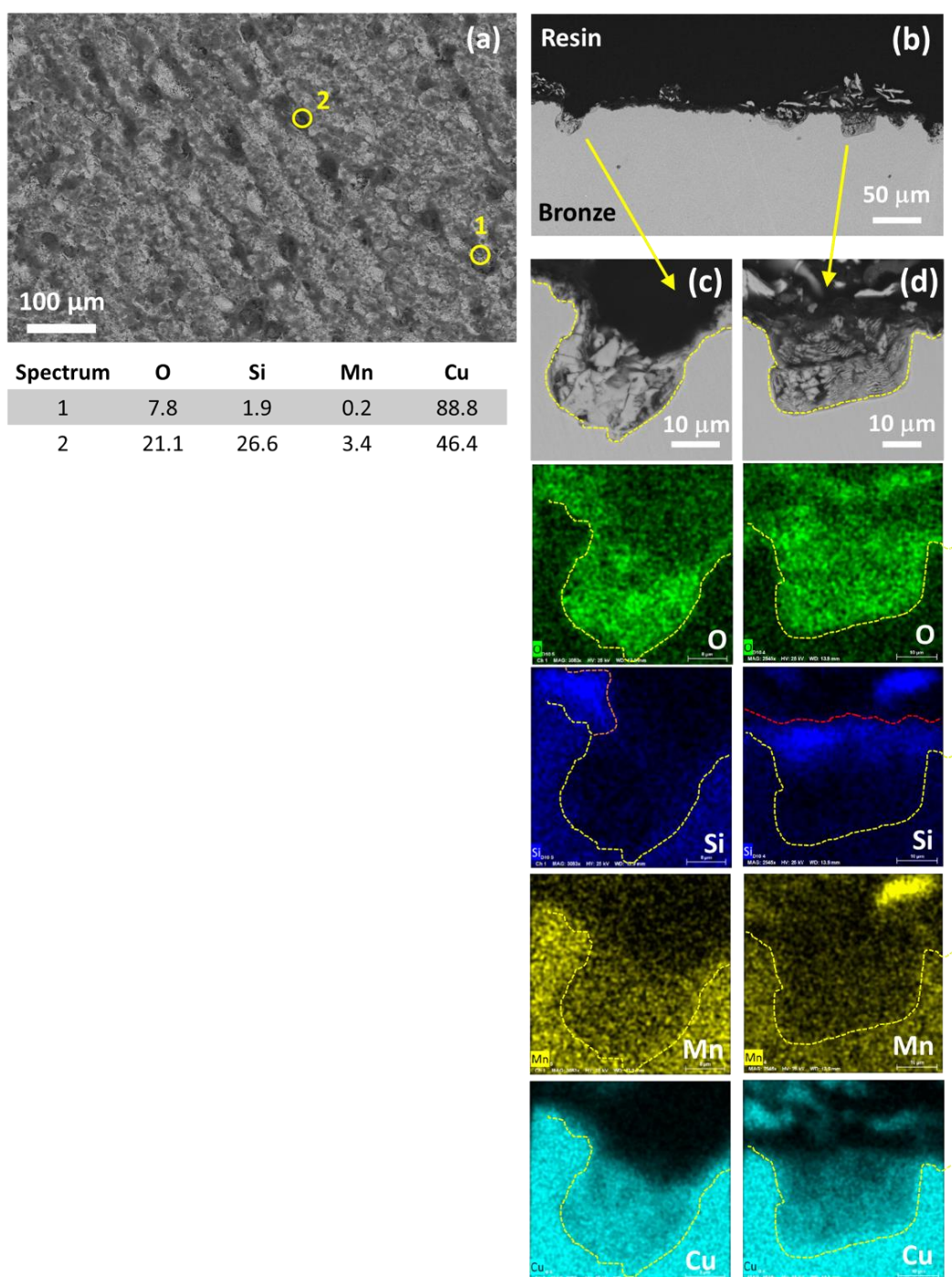


Figure 7: (a) BSE-SEM image of the surface (ToW=60 days) with indication of (1) non Si-enriched and (2) Si-enriched spots (as indicated by EDS wt% data reported below the micrograph) and (b) general view of the cross-section with (c) X-ray maps of a crater without Si-rich top layer; (d) X-ray maps of a crater with Si-rich top layer.

The corrosion patina appeared generally very thin ($< 2 \mu\text{m}$) and some detachments were locally observed as well as localised corrosion craters (Figure 7b). From a compositional point of view, in agreement with the surface analyses, the corrosion patina is characterised by Cu and O species (Figure 7c and d). Si maps collected in the two main types of craters show different features: one of them is covered by a continuous layer of Si-enriched products (Figure 7d), whilst in the other crater this continuous layer, still present at the border of the crater, is not present anymore above it (Figure 7c). This could suggest that a detachment of Si-rich corrosion products from the surface, due to runoff, is responsible for the differentiation among Si-enriched

and non-enriched areas observed on the surface, with dark spots of Figures 5 and 7 corresponding to craters with undetached Si-rich products still present above the crater. The localisation of corrosion attack which led to the formation of craters like those in Figure 7 is probably related to microstructural features such as the Si-rich micro-constituents in the interdendritic space, as demonstrated by the optical image of the etched cross-section in Figure 8.

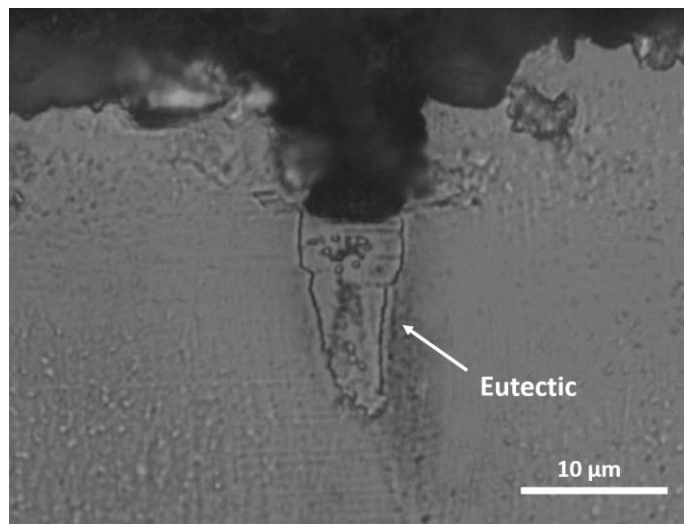


Figure 8: Optical micrograph (cross-section) of the Cu-3Si-1Mn bronze after 60 days of exposure by dropping test, showing the formation of a crater in correspondence with the Si-rich interdendritic micro-constituent (etching by FeCl_3/HCl).

The phase composition of the patina was investigated by micro-Raman and FTIR spectroscopy. The corrosion products detected by Raman mainly consisted of crystalline cuprous oxide. In addition, Raman bands at $770 - 790 \text{ cm}^{-1}$ [29], locally detected in correspondence with gel-like corrosion products, were attributed to the nSi-O-H symmetric stretch.

FTIR spectra collected on the corrosion products formed at 5 to 30 days of ToW are reported in Figure 9. Both of them exhibit the same peaks which appear more defined and intense at higher ToW. Therefore, in Table 3 the peak frequencies obtained from the FTIR spectra at 30 days of ToW are reported, together with their assignment. These data confirm the hypothesised formation of cuprite and a hydrated SiO_2 product on Cu-3Si-1Mn. Acetate and formate organic anions were clearly detected on the surface corrosion products. These anions, which are minor components of AR and tend to form soluble copper salts, are likely present as adsorbed species.

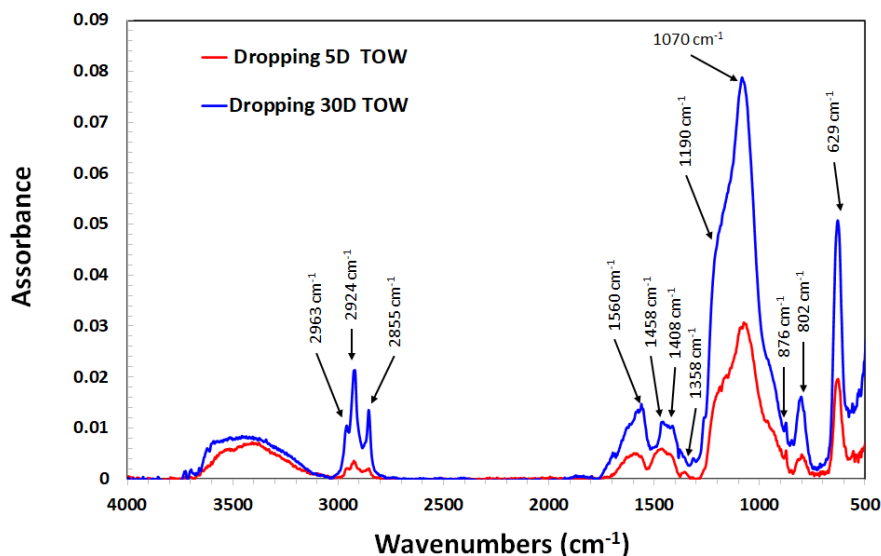


Figure 9: FTIR (applying DRIFT) spectra of corrosion products formed during accelerated ageing after 5 days and 30 days of ToW.

Table 3: FTIR vibrational bands detected on the corrosion products formed on Cu3-Si-1Mn during accelerated ageing.

Assignment	Vibration	Wavenumber/ cm^{-1}	Reference
Product hydration	O-H stretching	3200 – 3500	[30]
	C-H asym. stretching	2988	
	C-H sym. stretching	2941	
Adsorbed acetate	COO ⁻ asym. stretching	1600-1560	[31,32]
	CH ₃ asym. bending	1458	
	COO ⁻ sym stretching	~1410	
Adsorbed formate	C-H sym stretching	2855	
	COO ⁻ asym. stretching	1600	[33–35]
	COO ⁻ sym stretching	1360	
SiO₂ gel	Si–O–Si asym. stretching	1200-1000	[35,36]
	Si-OH sym. stretching	876	
Cu₂O	Cu(I)-O vibration	629	[37–39]

To obtain deeper structural information on the Si-enriched gel-like corrosion product, TEM-EDS analyses were carried out. The acquired lattice images showed an amorphous structure (Figure 10a) and a strong enrichment in Si was confirmed by localised EDS measurements (Figure 10b). These results are consistent with FTIR and Raman analyses. The observed gel-like morphology is similar to that observed in an outdoor quaternary bronze artefact, where a gel-like with nano-crystalline Sn-based compounds was detected [14].

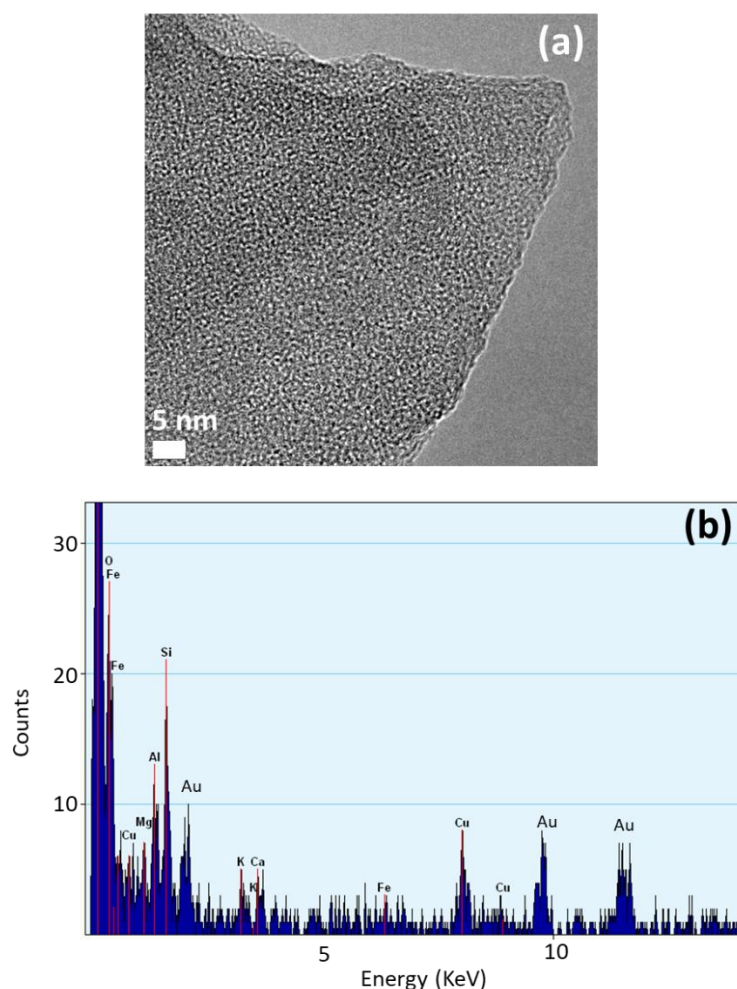


Figure 10: (a) TEM lattice image and (b) EDS spectra of the gel-like corrosion products collected in correspondence with dendrite borders.

Sulphur and nitrogen containing corrosion products were not detected by micro-Raman and FITR in these conditions. This is in agreement with the very low content of S and N revealed by EDS analyses. In fact, S was locally revealed only in very few points and always <1.5 wt%, while not significant amounts were recorded in the general EDS maps. As reported in previous papers [9,10,40], longer time are required for S-products to be formed under relatively low concentration of sulphate, representative of the present atmospheric conditions. Nitrogen containing corrosion products were never detected due to their high solubility.

3.3 Runoff accelerated ageing: Mass and thickness variation and corrosion rate

The above discussed results on corroded surfaces are also confirmed by mass and thickness variation evaluated as a function of ToW (Figure 11). Mass variation per unit of corroded area (Figure 11a) showed a global linear mass decrease (slope = -0.290; $r^2 > 0.99$) induced by the chemical and mechanical actions of the rain on the bronze surfaces. In particular, after 30 days of dropping, an average mass decrease of $8 \pm 2 \text{ mg/cm}^2$ was calculated and this value is comparable to that measured for Cu-5Sn-5Zn-5Pb quaternary bronze under the same conditions (between 8 and 10 mg/cm^2) [9,11].

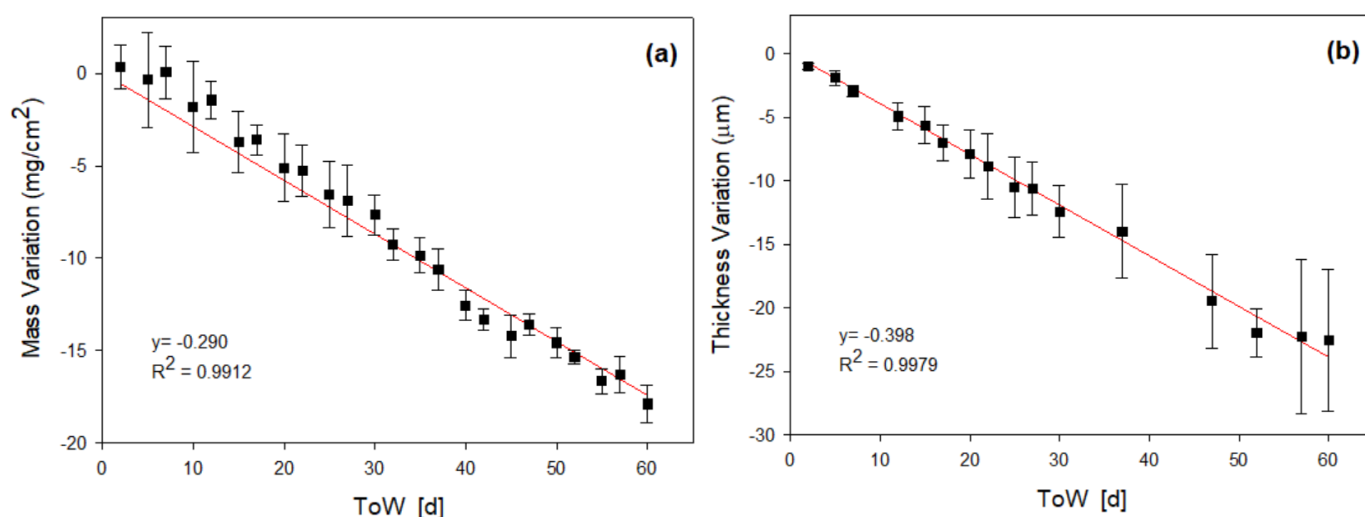


Figure 11: (a) Mass and (b) Thickness variations of Cu-3Si-1Mn bronze under dropping condition vs. time of wetness (ToW).

The average thickness variation trend (Figure 11b) linearly decreased with ToW and the final value was -23 ± 6 μm after 60 days of dropping. Finally, the corrosion rates of the alloy (v_{cor}) at both 30 and 60 days of ToW were calculated as thickness losses after pickling procedures. As expected from mass variation data evaluated without pickling, v_{cor} remained constant during the test and equal to 0.45 μm/day_{ToW}. Considering the density of the alloy (8.3 ± 0.3 mg/mm³), this value does not significantly differ from the gravimetric corrosion rate calculated from mass loss (0.37 ± 0.03 mg/cm² per day of ToW). This corrosion rate is comparable to v_{cor} of a Cu-5Sn-5Zn-5Pb exposed to dropping test for 30 days of ToW (around 0.45 μm/day_{ToW}) [9,11].

3.4 Runoff accelerated ageing: Metal release

The analysis of the alloy elements (Cu, Si and Mn) dissolved in the synthetic rain allowed to gain a more complete understanding of Cu-3Si-1Mn corrosion. Figure 12 reports the periodic (left-side column) and cumulative (right-side column) metal release as a function of ToW. Cu, as expected, is the most released metal and dissolves at a slightly increasing rate up to 15 days of ToW, then quite constantly up to 60 days of ToW. However, the overall cumulative Cu release increases almost linearly with time. Mn, after a high release during the first hours, exhibited a reduced dissolution rate up to 30 days of ToW, then a constant but slightly lower release until the end of the exposure. Therefore, its cumulative curve is a piecewise linear function with lower slope after 30 days of ToW. Si shows a completely different trend. Specifically, up to 10 days of ToW its concentration was under the limit of detection (when surface analyses showed a relative Si-enrichment, Figure 3b). Then, a progressive increase in Si release was observed up to 15-16 days of ToW, followed by a decrease until 30 days and finally by a constant release period: the corresponding cumulative curve has a logarithmic trend. This is in agreement with EDS results (Figure 6b), highlighting that after 10 days of ToW Si-based compounds formed during the first period start to detach from the patina. Then, the patina reaches a quasi-stationary condition with a constant and low Si release. The initial Si behaviour up to 10 days of ToW can be partially compared to that observed for Cu-5Sn-5Zn-5Pb, in which Sn produced adherent and insoluble corrosion products within the patina [9,11].

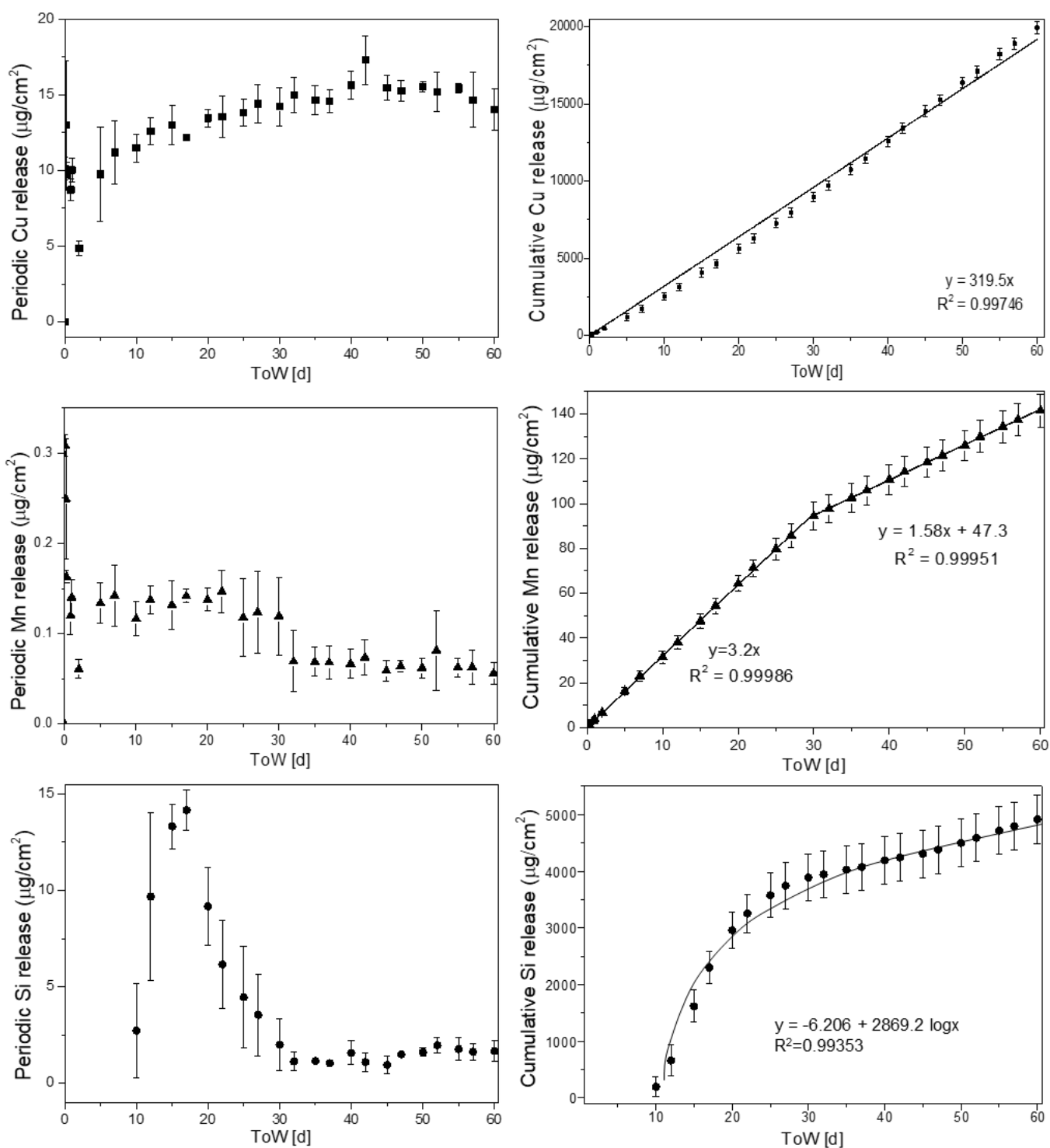


Figure 12: Periodic (left column) and cumulative (right column) values of the leached metallic cations (Cu, Si and Mn) as a function of the time of wetness (ToW).

Finally, in order to highlight possible preferential dissolution of alloying elements by comparison to Cu, the M/Cu ratio (M= Mn or Si) was normalised with respect to the same ratio in the alloy before ageing (EDS results in Figure 3, Table S1) (Figure 13). Si shows a highly preferential dissolution between 10 and 30 days

of ToW, then stabilises around values close to the ratio in the alloy, while Mn does not dissolve preferentially during exposure, apart from the first hours.

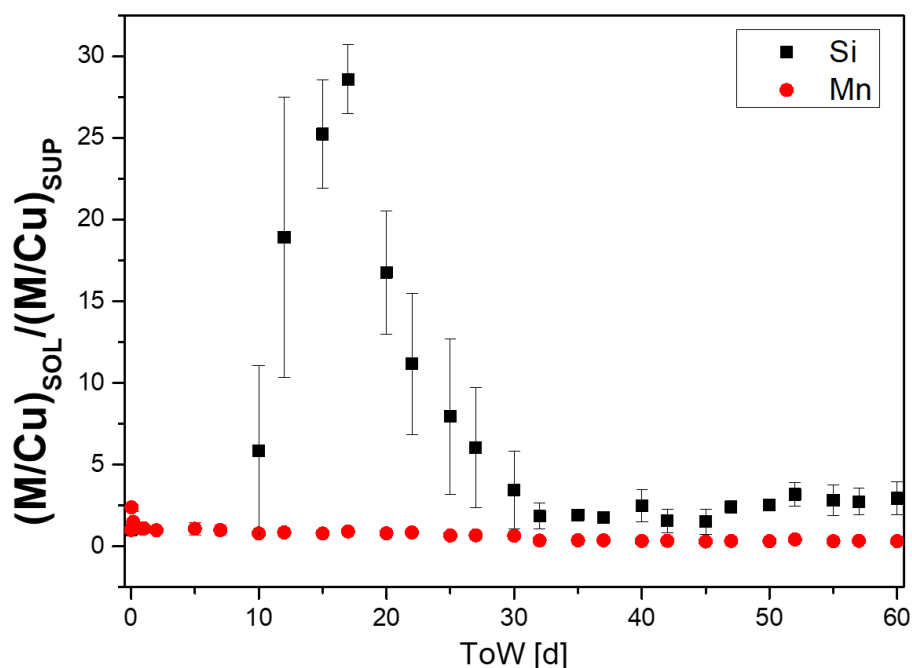


Figure 13: Ratio of Si and Mn released in solution by comparison to Cu, normalized considering the same ratio in the bulk alloy by EDS before accelerated ageing. Values are reported as a function of ToW.

3.5 Full immersion tests: surface characterisation

The corrosion behaviour of the Cu-3Si-1Mn and Cu-5Sn-5Zn-5Pb bronze was studied also in stagnant conditions, during 15 days of immersion in AR solution, to better understand the role of the alloying elements and surface patina, and gain a more complete understanding of their corrosion mechanisms. The evolution of the surface morphology and composition of the two bronzes was monitored by SEM/EDS during immersion tests (the results are reported in Figure S3 and Table S2 and S3).

Already after 1 day of immersion, the surface of the Cu-3Si-1Mn bronze is fairly uniformly covered with a layer of copper corrosion products (mainly Cu_2O): the inhomogeneities observed during exposure to dropping (Mn- and Si-rich areas) were not observed during full immersion tests (see Figure S3). During the exposure period (1-15 days), the corrosion product layer showed a constant oxygen concentration of about 10 wt% and was progressively depleted in Si (from 3.5 wt%, in the alloy, to 0.2 wt% after 15 days, likely due to the surface cathodic alkalization favoured by immersion under stagnant conditions) and Mn (from 0.8 to 0.4 wt% after 15 days of immersion). After 15 days of immersion, a more compact layer of cuprite is mainly formed in the dendritic areas (see Figure S4).

During full immersion tests the Cu-5Sn-5Zn-5Pb surface film underwent significant changes with time. C and O contents increased from 1 to 15 days (C = 4.7 wt% at 1 day, 8.0 wt% at 15 days; O = 6.7 wt% at 1 day, 9.6 wt% at 15 days). Zn was selectively dissolved (Zn = 4.6 wt% in the alloy, 0.8 wt% after 15 days), while Sn content increased from 5.1 wt% in the alloy to 5.4 wt% after 7 days of immersion, then decreased to 2.7 wt%. However, the Cu/Sn ratio continuously decreased from 16.6 in the alloy to 10.7 after 15 days, suggesting a relative surface enrichment in Sn due to the precipitation of insoluble and a partially protective tin oxide /oxyhydroxides (clearly evident in the Sn-rich interdendritic areas). Pb content increases from 3.7 wt% in the

alloy to 49.7 wt% on the surface after 15 days of immersion, due to the precipitation of hydrocerussite, $\text{Pb}_3(\text{CO}_3)_2(\text{OH})_2$, as revealed by XRD analysis (see Figure S5).

3.6 Full immersion tests: EIS measurements

The evolution of the corrosion behaviour of the studied bronzes was monitored by EIS during 15 days of immersion in AR solution. Selected impedance spectra are collected in Figure 14 in the Nyquist (Figure 14a and c) and Bode (phase angle, Figure 14b and d) representations for Cu-3Si-1Mn (Figure 14a and b) and the benchmark Cu-5Sn-5Zn-5Pb (Figure 14c and d).

As often found for copper and bronze exposed to mildly aggressive environments [41–44], three capacitive time constants were clearly detected in the spectra of the unleaded bronze at immersion times longer than 1 day. At shorter immersion times the High Frequency (HF) time constant was not evident (Figure 14a and b). The electrical equivalent circuits illustrated in Figure 15b and c, used to interpret the corrosion behaviour during the immersion period, were composed of two or three nested R-CPE couples, where:

- R_s represents the solution resistance between the bronze electrode and the reference electrode;
- the R_f - CPE_f couple describes the dielectric properties of a surface corrosion product film (HF time constant), with R_f and C_f corresponding to the resistance towards the access of ions through the film and the pseudocapacitance film;
- the R_t - CPE_{dl} couple is correlated to the charge transfer reaction occurring on bronze (medium frequency, MF, time constant) and R_t and C_{dl} are the charge transfer resistance and the capacitance of the double layer at the metal-electrolyte interface;
- the R_F - CPE_F pair (low frequency, LF, time constant) refers to the faradaic reactions of oxidation – reduction in the surface corrosion products (generally related to the redox reaction between Cu and Cu(I) ions, the latter incorporated into the Cu_2O -based surface film [45–47]); therefore R_F and C_F are the resistance of the faradaic reactions and the related pseudocapacitance value, respectively.

The constant phase elements (CPE) were used to consider the non-ideality associated with uneven current distribution due to surface roughness, formation of porous patina layers and variations in the properties or structures of the patina layer [46,47]. The impedance expression of CPE is:

$$Z = [Y(j \omega)^n]^{-1} \quad (1)$$

where $\omega = 2\pi f$ is the angular frequency (in rad s^{-1}), $j = \sqrt{-1}$ is the imaginary unit, Y is a frequency independent value (in $\text{ohm}^{-1} \text{cm}^{-2} \text{s}^n$) and n is a fit parameter with values in the range $-1 \leq n \leq 1$. The corresponding effective capacitances (C) were determined by the equation:

$$C = (R^{1-n} Y)^{1/n} \quad (2)$$

(valid for $0.54 \leq n \leq 0.99$), where R is the corresponding R-CPE couple resistance [48,49].

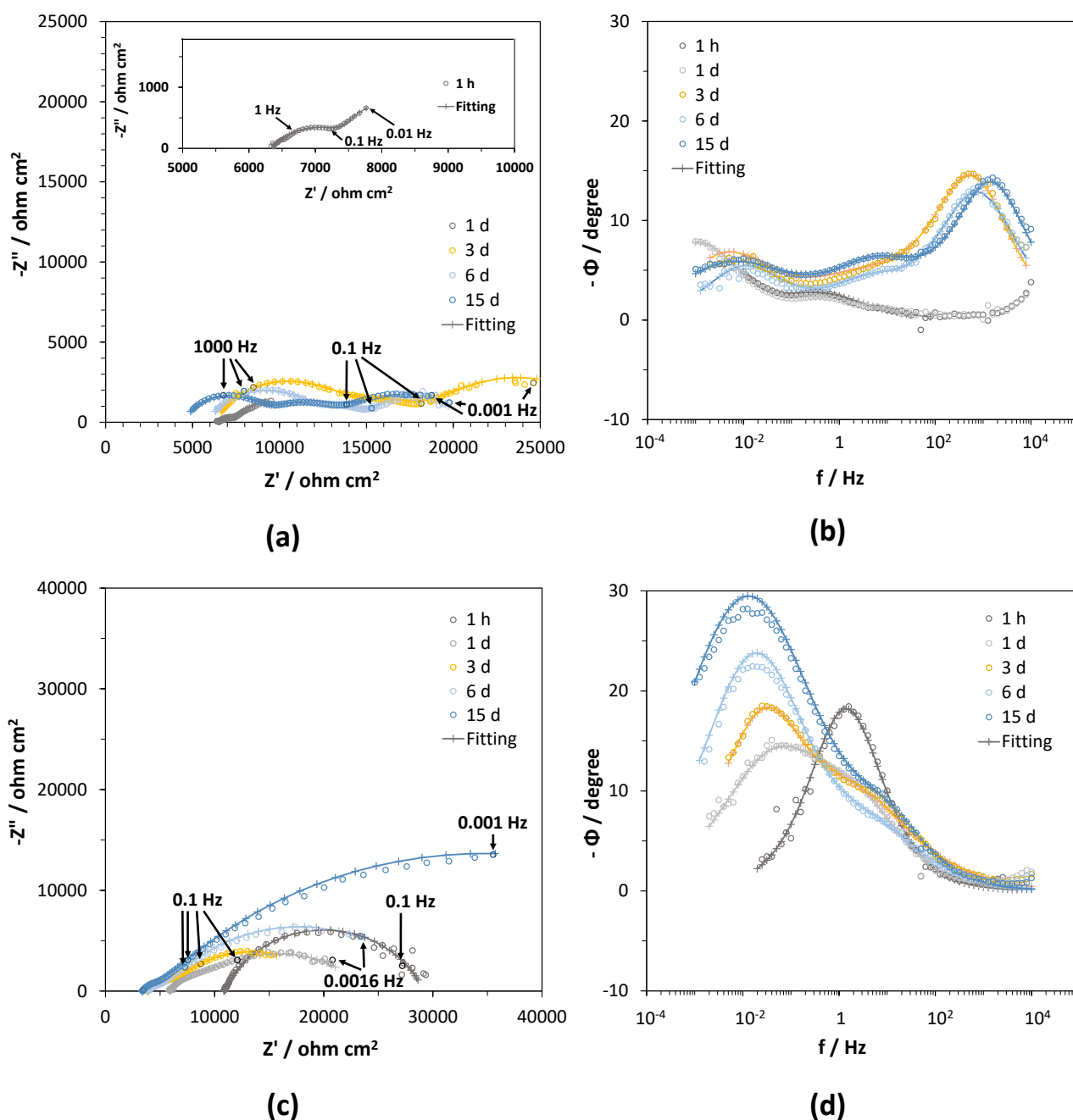


Figure 14: Nyquist (a,c) and Bode plots (phase angle, b,d) of the impedance spectra recorded on Cu-3Si-1Mn (a,b) and Cu-5Sn-5Zn-5Pb (c,d) bronze electrodes after different immersion times in AR. Circles correspond to measured data, while crosses and solid lines to the simulated results obtained by using the equivalent circuits depicted in Figure 15, as described in the text.

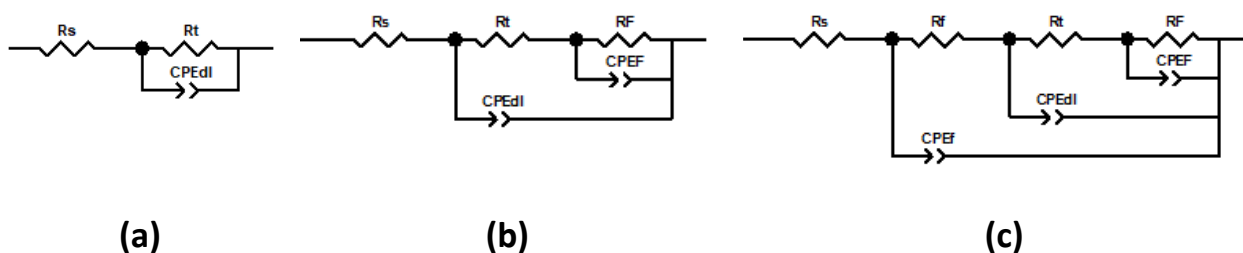


Figure 15: Equivalent circuits used to fit the experimental impedance spectra containing: (a) one, (b) two and (c) three time constants.

The time evolution of the parameters extracted by fitting of the spectra for Cu-3Si-1Mn are reported in Figure 16 (solid lines). Although the surface film characteristics, R_f and C_f , were only detected after 2 days of immersion, a thin surface film was present as detected by SEM-EDS after immersion periods of 1 ÷ 15 days. The patina evolution determined an initial R_f increase to 7500 ohm cm² (3 days), then oscillations around 4000 ohm cm², while the concomitant C_f values decreased from $6.8 \cdot 10^{-8}$ to $3.5 \cdot 10^{-8}$ F cm⁻² (Figure 16).

R_t and R_F values increased from 1 h to 3 days of immersion and then remained approximately constant with values comparable to each other and similar to R_f . Meanwhile, C_{dl} and C_F decreased during the initial 3 days, then reached plateaus. In particular, C_{dl} exhibited initial values of about $4.2 \cdot 10^{-4}$ F cm⁻² which decreased to $1.5 \cdot 10^{-5}$ F cm⁻², after 3 days of immersion. These values are compatible with double layer capacitances and confirm the validity of the equivalent circuit adopted. C_F showed much higher values, already detected in the case of redox reactions [45], that is $2.0 \cdot 10^{-2}$ F cm⁻² after 1 h which stabilised at $3 \cdot 5 \cdot 10^{-3}$ F cm⁻² during the immersion. The initial increase in R_t and decrease in C_{dl} could be connected to the growth of the thin surface film, which is reputed to reduce the metal/solution contact area, so hindering charge transfer. During the initial 3 days, R_F and C_F variations are indicative of a surface film stabilisation [49,50] which reduces the faradaic activity. Subsequently this activity does not change much, as suggested by the constancy of these parameters.

Similarly to Cu-3Si-1Mn, Cu-5Sn-5Zn-5Pb presented EIS spectra with a MF time constant connected to the charge transfer process and (at immersion times longer than 1h) a LF time constant due to a redox process in the corrosion products (Figure 16c and d). However, as already found by other authors investigating the corrosion behaviour of Cu-Sn and Cu-Sn-Pb alloys in acidic rain [44,46,51], the EIS spectra did not evidence the dielectric properties of the surface film, even if it was detected by SEM-EDS analyses. Therefore, they were fitted by the equivalent circuits in Figure 15a and b depending on the immersion time. It is possible that in this environment the film characteristic frequencies are higher than those accessible by our EIS instrumentation, due to the film relatively high conductivity [52].

The fitting parameters reported in Figure 16 show that on this bronze rather high initial R_t values were obtained ($2.0 \cdot 10^4$ ohm cm²) that decreased with time to $1.8 \cdot 10^3$ ohm cm². This suggests a progressive deterioration of the surface film which determined an easier access of the electrolyte to the metal surface and an easier support for electron transfer. C_{dl} increased a little up to 3 days of immersion (from $1.2 \cdot 10^{-5}$ to $4.6 \cdot 10^{-5}$ F cm⁻²) confirming the hypothesis of a slight increase in bronze surface area in contact with the solution, but subsequently this parameter oscillated coming back to the initial values. These trends were accompanied by a continuous increase in R_F values which can be attributed to a reduction in the surface film activity towards the redox reaction:



The findings are related to the modification of the initial Cu(I)-rich surface film, into a film of different nature, scarcely protective (as indicated by R_t and C_{dl} time trends) and characterised by a lower redox activity. During the immersion, the Cu-5Sn-5Zn-5Pb bronze surface is progressively covered by insoluble Sn oxide/oxyhydroxide and Pb corrosion products, as revealed by SEM-EDS analyses which detected an enrichment in Sn and, particularly, Pb.

The concomitant CF increase detected was likely due to a significant ion adsorption (Figure 14c).

Figure 16d collects the time evolution of E_{cor} and the polarisation resistance (R_p), evaluated as the sum of the three following contributes [42,43,49,53]:

$$R_p = R_f + R_t + R_F \quad 3)$$

Cu-3Si-1Mn exhibited low initial R_p values of about $2.9 \cdot 10^3$ ohm cm^2 which increased to $2.3 \cdot 10^4$ ohm cm^2 after 3 days of immersion and then decreased to a final value of about $1.7 \cdot 10^4$ ohm cm^2 . These values resulted almost always lower than those of the reference Cu-5Sn-5Zn-5Pb bronze (from $2.0 \cdot 10^4$ to $6.2 \cdot 10^4$ ohm cm^2 at the end of the immersion period) indicating for the later a slightly lower corrosion rate.

The highest R_p values of Cu-5Sn-5Zn-5Pb are mainly dominated by the higher R_F values, suggesting that, in stagnant conditions the Sn and Pb-rich corrosion layer can slow down the overall corrosion processes.

These results appear in disagreement with those obtained in [2,3,4] showing better corrosion performances of Si bronze in comparison to traditional CuSnZnPb alloys. However, the silicon bronzes studied in these works showed a high Sn content (8-10 wt%) and certainly, as observed in this study, the formation of a surface film rich of tin corrosion products contributed to these positive results.

The E_{cor} values of the studied Cu-3Si-1Mn bronze did not change very much during the immersion period and remained always close to or somewhat higher than the Cu/Cu₂O equilibrium potential calculated at pH 4.35 (-0.025 V_{SCE} at 25 °C), confirming the thermodynamic stability of Cu₂O on the electrode surface. Less noble initial E_{cor} values were detected on the reference Cu-5Sn-5Zn-5Pb (-0.081 V_{SCE}) which quickly ennobled to 0.008 V_{SCE} after 1 day of immersion and reached a value of $+0.068$ V_{SCE} at the end of the immersion period, likely suggesting a progressively lower anodic activity of this bronze, in turn connected to a lower faradaic activity (high R_F values) of the surface film.

In fact, on this bronze the low faradaic activity tends to control the alloy corrosion rate, by hindering the overall sequence of reactions A) and B) [44,54], as also highlighted by EIS analysis:



These results show that, in less aggressive stagnant conditions (full immersion), without the mechanical action of AR dropping, Cu-5Sn-5Zn-5Pb resulted slightly more corrosion resistant than the modern Cu-3Si-1Mn (Figure 16d). This is due to the growth of a complex film, rich in insoluble Sn and Pb corrosion products, on the Cu-5Sn-5Zn-5Pb surface. This film is quite stable in the stagnant condition and is able to reduce the overall corrosion rate.

Under more aggressive runoff condition, where both mechanical and chemical action may occur, on Cu-5Sn-5Zn-5Pb, the Pb-rich film was not observed as the leaching conditions do not allow to reach the solubility limit for its precipitation. Moreover, the dropping mechanical action probably damages the Sn-rich film, making it less stable and protective. Under this exposure condition, the corrosion rate of the studied alloys turned out to be comparable, also because the gel-like Si-rich film formed on Cu-3Si-1Mn is barely protective.

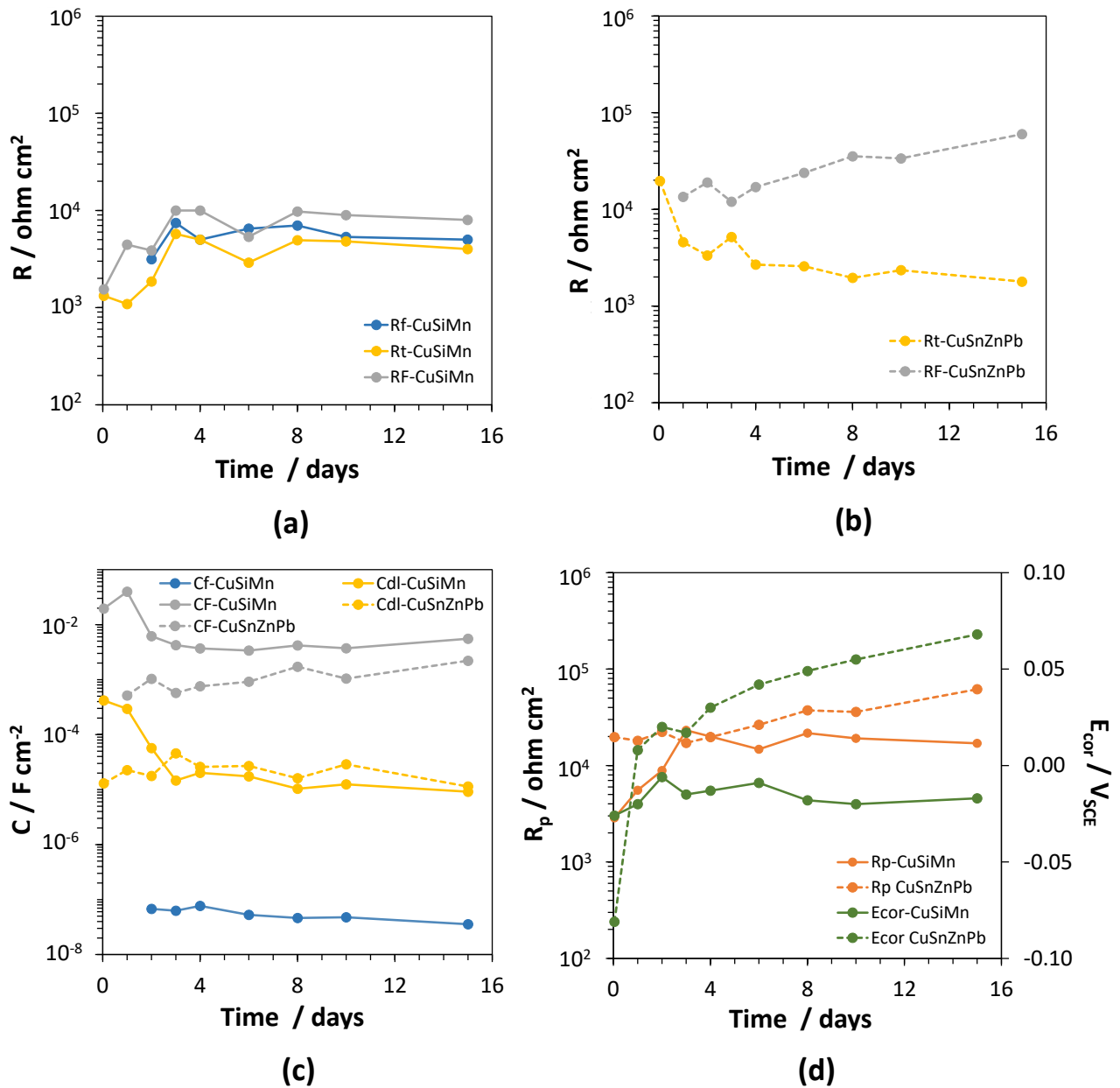


Figure 16: Time evolution of the electrochemical impedance parameters and E_{cor} for Cu-3Si-1Mn (solid lines) and Cu-5Sn-5Zn-5Pb (dotted lines) bronze during immersion in AR.

4. Conclusions

Atmospheric corrosion of the Pb-free Cu-3Si-1Mn bronze used for contemporary art was investigated by continuous immersions in synthetic acid rain (AR) as well as by accelerated ageing tests (AR dropping) simulating continuous runoff of the bronze surfaces. A traditional quaternary leaded bronze used for artistic casting (Cu-5Sn-5Zn-5Pb) was used as a reference for comparison and discussion of corrosion results. The following conclusions can be drawn:

- During runoff, the presence of heterogeneous microconstituents in interdendritic areas leads to localised corrosion, inducing the formation of craters, from which Si-rich layers (consisting of hydrated SiO_2 products) may detach, enhancing metal release in the first steps of accelerated ageing. Cu-3Si-1Mn

surface tends to become depleted in Cu and Mn and enriched in Si (which slightly decreased, then stabilised). The corrosion patina was generally very thin ($< 2 \mu\text{m}$), mainly composed by crystalline cuprous oxide and amorphous Si products. Si-rich corrosion products start to detach only after 10 days of ToW, then Si preferentially dissolves and finally stabilises around values close to the ratio in the alloy reaching a quasi-stationary condition with a constant and low Si release. In runoff conditions, where the mechanical action plays a role, the corrosion resistance in terms of thickness loss is $v_{\text{cor}} \sim 0.45 \mu\text{m/day}_{\text{ToW}}$, comparable to that of the traditional Cu-5Sn-5Zn-5Pb alloy.

- During continuous immersion, the Cu-3Si-1Mn surface is uniformly covered by a film of copper corrosion products, more compact in the dendritic areas, and becomes progressively depleted in Si and Mn. The Cu-5Sn-5Zn-5Pb bronze shows a selective Zn dissolution and a relative Sn enrichment, due to the precipitation of insoluble and partially protective tin oxide/oxyhydroxides. A strong Pb increase was detected on the surface as a result of Pb corrosion products precipitation (hydrocerussite) during immersion. The electrochemical tests performed on both Cu-3Si-1Mn and Cu-5Sn-5Zn-5Pb bronzes during continuous immersion revealed that the Pb-free modern alloy is slightly less corrosion resistant than the traditional one, due to the formation of Sn and Pb rich corrosion products, on the latter. With respect to Sn oxide and hydroxide, whose solubility is very low, Si tends to form less protective hydrated amorphous corrosion products. The corrosion rate of the Cu-5Sn-5Zn-5Pb alloy is limited by the low redox activity of the surface film, while the corrosion resistance of the modern Pb-free alloy is due to equivalent contributes from film resistance, charge transfer resistance and faradaic reaction resistance.

Acknowledgment

This paper is dedicated to the beloved memory of Cecilia Monticelli (1958-2022), Professor of Corrosion Science at the University of Ferrara (Italy), our friend and colleague who unfortunately left us all too early. We will never forget the years we spent at her side and her extraordinary professionalism, competence and dedication.

The authors would acknowledge Livartis d.o.o. (Slovenia) for having produced silicon bronze coupons within the M-ERA.NET European B-IMPACT project (www.b-impact.cloud).

Funding

This research did not receive any specific grant from funding agencies in the public, commercial, or not-for-profit sectors.

Data availability

The raw/processed data required to reproduce these findings cannot be shared at this time as the data also forms part of an ongoing study.

References

- [1] F. Gallese, G. Laguzzi, L. Luvidi, V. Ferrari, S. Takacs, G. Venturi Pagani Cesa, Comparative investigation into the corrosion of different bronze alloys suitable for outdoor sculptures, *Corros. Sci.* 50 (2008) 954–961. <https://doi.org/10.1016/j.corsci.2007.11.015>.
- [2] G.L. Garagnani, F. Piasentini, G. Venturi Pagani Cesa, Caratterizzazione microstrutturale e meccanica di leghe di rame da fonderia per applicazioni artistiche, *La Metall. Ital.* (2006) 39–46.
- [3] C. Chiavari, A. Colledan, A. Frignani, G. Brunoro, Corrosion evaluation of traditional and new bronzes for artistic castings, *Mater. Chem. Phys.* 95 (2006) 252–259. <https://doi.org/10.1016/j.matchemphys.2005.06.034>.
- [4] E. Švara Fabjan, T. Kosec, V. Kuhar, A. Legat, Corrosion stability of different bronzes in simulated Urban rain, *Mater. Tehnol.* 45 (2011) 585–591.
- [5] E. Bernardi, C. Chiavari, C. Martini, L. Morselli, The atmospheric corrosion of quaternary bronzes: An evaluation of the dissolution rate of the alloying elements, *Appl. Phys. A.* 92 (2008) 83–89. <https://doi.org/10.1007/s00339-008-4451-0>.
- [6] C. Debiemme-Chouvy, F. Ammeloot, E.M.M. Sutter, X-ray photoemission investigation of the corrosion film formed on a polished Cu-13Sn alloy in aerated NaCl solution, *Appl. Surf. Sci.* 174 (2001) 55–61.
- [7] I. Mabile, A. Bertrand, E.M.M. Sutter, C. Fiaud, Mechanism of dissolution of a Cu-13Sn alloy in low aggressive conditions, *Corros. Sci.* 45 (2003) 855–866. [https://doi.org/10.1016/S0010-938X\(02\)00207-X](https://doi.org/10.1016/S0010-938X(02)00207-X).
- [8] S. Goidanich, I. Odnevall Wallinder, G. Herting, C. Leygraf, Corrosion induced metal release from copper based alloys compared to their pure elements, *Corros. Eng. Sci. Technol.* 43 (2008) 134–141. <https://doi.org/10.1179/174327808X286383>.
- [9] E. Bernardi, C. Chiavari, B. Lenza, C. Martini, L. Morselli, F. Ospitali, L. Robbiola, The atmospheric corrosion of quaternary bronzes: The leaching action of acid rain, *Corros. Sci.* 51 (2009) 159–170. <https://doi.org/10.1016/j.corsci.2008.10.008>.
- [10] C. Chiavari, E. Bernardi, C. Martini, F. Passarini, F. Ospitali, L. Robbiola, The atmospheric corrosion of quaternary bronzes: The action of stagnant rain water, *Corros. Sci.* 52 (2010) 3002–3010. <https://doi.org/10.1016/j.corsci.2010.05.013>.
- [11] C. Chiavari, E. Bernardi, C. Martini, L. Morselli, F. Ospitali, L. Robbiola, A. Texier, Predicting the corrosion behaviour of outdoor bronzes: assessment of artificially exposed and real outdoor samples, *Met. 2010 Proc. Interim Meet. ICOM-CC Met. Work. Group*, Oct. 11-15, 2010, Charleston, South Carolina, USA. (2011) 218–226.
- [12] G. Masi, J. Esvan, C. Josse, C. Chiavari, E. Bernardi, C. Martini, M.C. Bignozzi, N. Gartner, T. Kosec, L. Robbiola, Characterization of typical patinas simulating bronze corrosion in outdoor conditions, *Mater. Chem. Phys.* 200 (2017) 308–321. <https://doi.org/10.1016/j.matchemphys.2017.07.091>.
- [13] L. Robbiola, K. Rahmouni, C. Chiavari, C. Martini, D. Prandstraller, A. Texier, H. Takenouti, P. Vermaut, New insight into the nature and properties of pale green surfaces of outdoor bronze monuments, *Appl. Phys. A Mater. Sci. Process.* 92 (2008) 161–169. <https://doi.org/10.1007/s00339-008-4468-4>.
- [14] C. Chiavari, K. Rahmouni, H. Takenouti, S. Joiret, P. Vermaut, L. Robbiola, Composition and electrochemical properties of natural patinas of outdoor bronze monuments, *Electrochim. Acta.* 52 (2007) 7760–7769. <https://doi.org/10.1016/j.electacta.2006.12.053>.

- [15] A. Cohen, Properties of Cast Copper Alloys, in: ASM Handbook Vol 2, Properties and Selection: Nonferrous Alloys and Special-Purpose Materials, (1990) 356–391.
- [16] K.C. Nnakwo, C.N. Mbah, C.C. Daniel-Mkpume, Investigation of the structural sensitive behavior of Cu-3Si-xMn ternary alloys, J. King Saud Univ. - Sci. 31 (2019) 1056–1063. <https://doi.org/10.1016/j.jksus.2019.01.001>.
- [17] V. Sastri, Corrosion of permanent mould cast copper alloys in aqueous solutions, Corros. Eng. Sci. Technol. 40 (2005) 65–68. <https://doi.org/10.1179/174327805X29868>.
- [18] N. Bantz, Failure of silicon bronze impeller from dealloying via desiliconification, J. Fail. Anal. Prev. 13 (2013) 545–550. <https://doi.org/10.1007/s11668-013-9732-z>.
- [19] A. Aravind, R. Saravanan, Improvement in hardness, wear rate and corrosion resistance of silicon bronze using gas tungsten arc, in: Mater. Today Proc., 2020. <https://doi.org/10.1016/j.matpr.2020.04.292>.
- [20] G. Masi, C. Josse, J. Esvan, C. Chiavari, E. Bernardi, C. Martini, M.C. Bignozzi, C. Monticelli, F. Zanotto, A. Balbo, E. Svara Fabjan, T. Kosec, L. Robbiola, Evaluation of the protectiveness of an organosilane coating on patinated Cu-Si-Mn bronze for contemporary art, Prog. Org. Coatings. 127 (2019) 286–299. <https://doi.org/10.1016/j.porgcoat.2018.11.027>.
- [21] Casting of Copper and Copper Alloys Casting, Vol 15, in: ASM Handbook, ASM Int., 2008: pp. 1026–1048.
- [22] G. Luciano, P. Traverso, P. Letardi, Applications of chemometric tools in corrosion studies, Corros. Sci. 52 (2010) 2750–2757. <https://doi.org/10.1016/j.corsci.2010.05.016>.
- [23] K. Varmuza, P. Filzmoser, Multivariate Statistical Analysis in Chemometrics, CRC Press, Taylor & Francis Group, 2009.
- [24] ISO 8407:2009(E), Corrosion of metal and alloys – Removal of corrosion products from corrosion test specimens, (2009).
- [25] J. Miettinen, Thermodynamic description of the Cu-Mn-Si system in the copper-rich corner, Comput. Coupling Phase Diagrams Thermochem. 27 (2003) 395–401. <https://doi.org/10.1016/j.calphad.2004.01.002>.
- [26] H. Turhan, M. Aksoy, V. Kuzucu, M.M. Yıldırım, The effect of manganese on the microstructure and mechanical properties of leaded-tin bronze, J. Mater. Process. Technol. 114 (2001) 207–211.
- [27] D. Rai, M. Yui, H.T. Schaef, A. Kitamura, Thermodynamic model for SnO₂(cr) and SnO₂(am) solubility in the aqueous Na⁺-H⁺-OH⁻-Cl⁻-H₂O system, J. Solution Chem. 40 (2011) 1155–1172. <https://doi.org/10.1007/s10953-011-9723-1>.
- [28] G. Charlot, Les reactions chimiques en solution, Masson et Cie, 1977.
- [29] P.K. Dutta, D.-C. Shieh, Raman Spectral Study of the Composition of Basic Silicate Solutions, Appl. Spectrosc. 39 (1985) 343–346. <https://doi.org/10.1366/0003702854248971>.
- [30] D. Mikić, H. Čurković, T. Kosec, N. Peko, An Electrochemical and Spectroscopic Study of Surfaces on Bronze Sculptures Exposed to Urban Environment, Mater. 2021, Vol. 14, Page 2063. 14 (2021) 2063. <https://doi.org/10.3390/MA14082063>.
- [31] J. Buse, V. Otero, M. Melo, New Insights into Synthetic Copper Greens: The Search for Specific Signatures by Raman and Infrared Spectroscopy for Their Characterization in Medieval Artworks, Heritage. 2 (2019) 1614–1629. <https://doi.org/10.3390/HERITAGE2020099>.

- [32] I. Bae, D. Scherson, E. Yeager, Infrared spectroscopic determination of pH changes in diffusionally decoupled thin-layer electrochemical cells, *Anal. Chem.* 62 (1990) 45–49. <https://doi.org/10.1021/ac00200a009>.
- [33] G. Millar, C. Rochester, K. Waugh, An FTIR Study of the Adsorption of Formic Acid and Formaldehyde on Potassium-Promoted Cu/SiO₂ Catalysts, *J. Catal.* 155 (1995) 52–58. <https://doi.org/10.1006/JCAT.1995.1187>.
- [34] P. Mitchell, R. Holroyd, S. Poulston, M. Bowker, S. Parker, Inelastic neutron scattering of model compounds for surface formates Potassium formate, copper formate and formic acid, *J. Chem. Soc. Faraday Trans. 93* (1997) 2569–2575. <https://doi.org/10.1039/A701231D>.
- [35] D. Lin-Vien, N.B. Colthup, W.G. Fateley, J.G. Grasselli, *The Handbook of infrared and raman characteristic frequencies of organic molecules*, Academic Press Inc., San Diego, CA, 1991.
- [36] C. Chiavari, A. Balbo, E. Bernardi, C. Martini, F. Zanotto, I. Vassura, M.C. Bignozzi, C. Monticelli, Organosilane coatings applied on bronze: Influence of UV radiation and thermal cycles on the protectiveness, *Prog. Org. Coatings.* 82 (2015) 91–100. <https://doi.org/10.1016/j.porgcoat.2015.01.017>.
- [37] Y. Zhang, J. Tang, G. Wang, M. Zhang, X. Hu, Facile synthesis of submicron Cu₂O and CuO crystallites from a solid metallorganic molecular precursor, *J. Cryst. Growth.* 294 (2006) 278–282. <https://doi.org/10.1016/J.JCRYSGRO.2006.06.038>.
- [38] M. Kooti, L. Matouri, Fabrication of Nanosized Cuprous Oxide Using Fehling's Solution, *Sci. Iran.* 17 (2010).
- [39] T. Chang, G. Herting, Y. Jin, C. Leygraf, I. Odnevall Wallinder, The golden alloy Cu₅Zn₅Al₁Sn: Patina evolution in chloride-containing atmospheres, *Corros. Sci.* 133 (2018) 190–203. <https://doi.org/10.1016/J.CORSCI.2018.01.027>.
- [40] A. Kratschmer, I. Odnevall Wallinder, C. Leygraf, The evolution of outdoor copper patina, 44 (2002) 425–450.
- [41] A. Dermaj, N. Hajjaji, S. Joiret, K. Rahmouni, A. Srhiri, H. Takenouti, V. Vivier, Electrochemical and spectroscopic evidences of corrosion inhibition of bronze by a triazole derivative, *Electrochim. Acta.* 52 (2007) 4654–4662. <https://doi.org/10.1016/J.ELECTACTA.2007.01.068>.
- [42] T. Wang, J. Wang, Y. Wu, The inhibition effect and mechanism of L-cysteine on the corrosion of bronze covered with a CuCl patina, *Corros. Sci.* 97 (2015) 89–99. <https://doi.org/10.1016/j.corsci.2015.04.018>.
- [43] C. Monticelli, A. Balbo, J. Esvan, C. Chiavari, C. Martini, F. Zanotto, L. Marvelli, L. Robbiola, Evaluation of 2-(salicylideneimino) thiophenol and other Schiff bases as bronze corrosion inhibitors by electrochemical techniques and surface analysis, *Corros. Sci.* 148 (2019) 144–158. <https://doi.org/10.1016/J.CORSCI.2018.12.017>.
- [44] S. Varvara, G. Caniglia, J. Izquierdo, R. Bostan, L. Găină, O. Bobis, R. Souto, Multiscale electrochemical analysis of the corrosion control of bronze in simulated acid rain by horse-chestnut (*Aesculus hippocastanum* L.) extract as green inhibitor, *Corros. Sci.* 165 (2020) 108381. <https://doi.org/10.1016/J.CORSCI.2019.108381>.
- [45] W. Qafsaoui, M. Kendig, H. Perrot, H. Takenouti, Coupling of electrochemical techniques to study copper corrosion inhibition in 0.5 mol L⁻¹ NaCl by 1-pyrrolidine dithiocarbamate, *Electrochim. Acta.* 87 (2013) 348–360. <https://doi.org/10.1016/J.ELECTACTA.2012.09.056>.
- [46] S. Varvara, R. Bostan, O. Bobis, L. Găină, F. Popa, V. Mena, R. Souto, Propolis as a green corrosion

inhibitor for bronze in weakly acidic solution, *Appl. Surf. Sci.* 426 (2017) 1100–1112. <https://doi.org/10.1016/J.APSUSC.2017.07.230>.

- [47] J. Wu, J. Wang, The effects of UV and visible light on the corrosion of bronze covered with an oxide film in aqueous solution, *Corros. Sci.* 154 (2019) 144–158. <https://doi.org/10.1016/J.CORSCI.2019.01.009>.
- [48] G. Brug, A. van den Eeden, M. Sluyters-Rehbach, J. Sluyters, The analysis of electrode impedances complicated by the presence of a constant phase element, *J. Electroanal. Chem. Interfacial Electrochem.* 176 (1984) 275–295. [https://doi.org/10.1016/S0022-0728\(84\)80324-1](https://doi.org/10.1016/S0022-0728(84)80324-1).
- [49] R. Bostan, S. Varvara, L. Gâinâ, L. Mureşan, Evaluation of some phenothiazine derivatives as corrosion inhibitors for bronze in weakly acidic solution, *Corros. Sci.* 63 (2012) 275–286. <https://doi.org/10.1016/J.CORSCI.2012.06.010>.
- [50] L. Muresan, S. Varvara, E. Stupnišek-Lisac, H. Otmačić, K. Marušić, S. Horvat-Kurbegović, L. Robbiola, K. Rahmouni, H. Takenouti, Protection of bronze covered with patina by innocuous organic substances, *Electrochim. Acta.* 52 (2007) 7770–7779. <https://doi.org/10.1016/j.electacta.2007.02.024>.
- [51] S. Varvara, L. Muresan, K. Rahmouni, H. Takenouti, Evaluation of some non-toxic thiadiazole derivatives as bronze corrosion inhibitors in aqueous solution, *Corros. Sci.* 50 (2008) 2596–2604. <https://doi.org/10.1016/J.CORSCI.2008.06.046>.
- [52] M.E. Orazem, B. Tribollet, *Electrochemical Impedance Spectroscopy*, John Wiley & Sons, Inc., Pennington, NJ, 2008. <https://doi.org/10.1002/9780470381588>.
- [53] K. Rahmouni, H. Takenouti, N. Hajjaji, A. Srhiri, L. Robbiola, Protection of ancient and historic bronzes by triazole derivatives, *Electrochim. Acta.* 54 (2009) 5206–5215. <https://doi.org/10.1016/j.electacta.2009.02.027>.
- [54] K. Marušić, H. Ćurković, H. Takenouti, Inhibiting effect of 4-methyl-1-p-tolylimidazole to the corrosion of bronze patinated in sulphate medium, *Electrochim. Acta.* 56 (2011) 7491–7502. <https://doi.org/10.1016/J.ELECTACTA.2011.06.107>.

Supplementary material for the manuscript:

Atmospheric corrosion of Cu-Si-Mn bronze for contemporary art under simulated runoff and continuous immersion conditions

Cristina Chiavari¹, Carla Martini², Andrea Balbo³, Cecilia Monticelli³, Cecilia Velino⁴, Giulia Masi⁵, Elena Bernardi^{4*}

¹Department for Cultural Heritage, University of Bologna, via degli Ariani 1, Ravenna, Italy, cristina.chiavari@unibo.it

²Department of Industrial Engineering, University of Bologna, viale Risorgimento 4, 40136 Bologna, Italy, carla.martini@unibo.it

³Centro di Studi sulla Corrosione e Metallurgia "A. Daccò", Tecnopolo di Ferrara, Department of Engineering, University of Ferrara, via Saragat 4A, 44122 Ferrara, Italy, andrea.balbo@unife.it

⁴Department of Industrial Chemistry "Toso Montanari", University of Bologna, viale Risorgimento 4, 40136 Bologna, Italy, elena.bernardi@unibo.it, cecilia.velino2@unibo.it

⁵Department of Civil, Chemical, Environmental and Materials Engineering, University of Bologna, via Terracini 28, 40131 Bologna, Italy, giulia.masi5@unibo.it

Figure S1	<i>Optical images (bright field) showing the microstructure of the Cu-3Si-1Mn alloy (etching by FeCl₃/HCl)</i>	<i>pag.2</i>
Table S1	<i>Elemental analysis (wt%) of the corroded surfaces at different time of exposure measured by EDS on large areas.....</i>	<i>pag.3</i>
Figure S2	<i>(a) Loading and Score plot for PC1 and PC2 of the PCA model related to the EDS analyses of dark spots on the surface as a function of ToW. (b) PC2 Scores plotted as a function of ToW of the related objects.....</i>	<i>pag.4</i>
Figure S3	<i>SEM-BSE images of Cu-3Si-1Mn and Cu-5Sn-5Zn-5Pb after immersions of 1, 7 and 15 days in artificial acid rain.....</i>	<i>pag.5</i>
Table S2	<i>SEM-EDS analyses (expressed in wt%) carried out on of Cu-3Si-1Mn after immersions of 1, 7 and 15 days in artificial acid rain</i>	<i>pag.6</i>
Table S3	<i>SEM-EDS analyses carried out on of Cu-5Sn-5Zn-5Pb after immersions of 1, 7 and 15 days in artificial acid rain</i>	<i>pag.6</i>
Figure S4	<i>SEM-BSE images of Cu-3Si-1Mn bronze after 15 days of immersion in artificial acid rain.....</i>	<i>pag.7</i>
Figure S5	<i>X-ray diffraction (XRD) patterns of patina formed on Cu-5Sn-5Zn-5Pb quaternary bronze surface after 15 days of immersion in artificial acid rain.</i>	<i>pag.7</i>

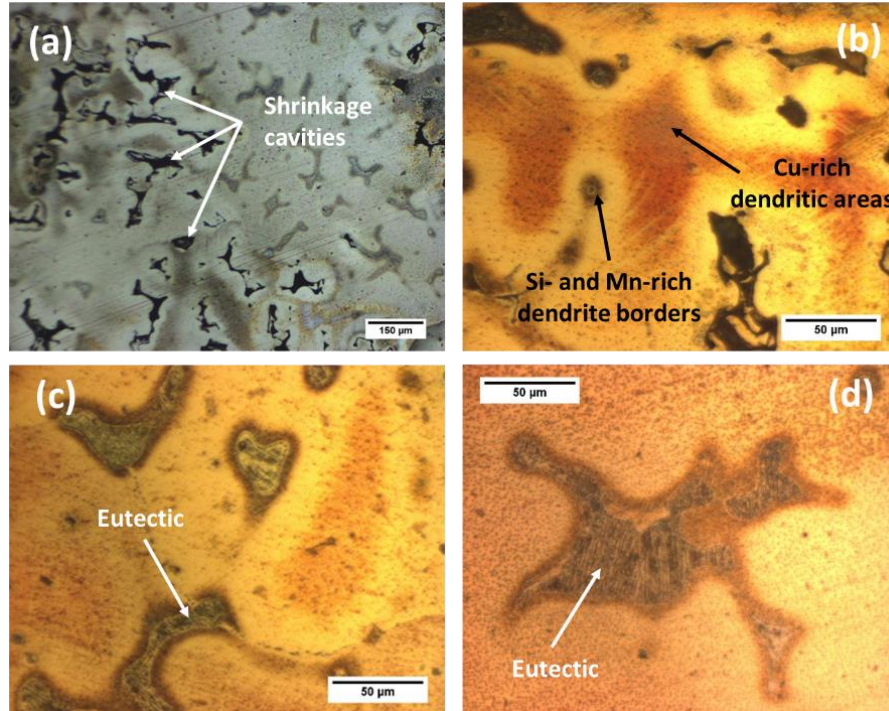


Figure S1: Optical images (bright field) showing the microstructure of the Cu-3Si-1Mn alloy (etching by FeCl_3/HCl).

Figure S1 shows a dendritic structure with shrinkage cavities in interdendritic spaces (a). Marked micro-segregation (i.e., coring) is also evident (b), leading to Si and Mn enrichment at dendrite borders, where a heterogeneous microstructural constituent is detected (c and d). This micro-constituent is characterised by a lamellar morphology (d) and can be ascribed to an eutectic phase transformation.

Table S1: Elemental analysis (wt%) of the corroded surfaces at different time of exposure measured by EDS on large areas (average values and standard deviations). The Cu/Si and Mn/Si ratios (wt%/wt%) with related error are also reported.

<i>ToW [days]</i>	<i>C*</i>	<i>O</i>	<i>Si</i>	<i>Mn</i>	<i>Cu</i>	<i>Cu/Si</i>	<i>Mn/Si</i>
0	8±1	2.1±0.3	3.5±0.1	1.1±0.1	85±1	24.3±0.8	0.31±0.01
2	5±2	14±4	4.5±0.9	0.9±0.1	75±3	17±3	0.20±0.04
5	5±1	16±5	6±2	0.8±0.1	68±10	11±4	0.13±0.05
10	5±1	21±4	7±3	0.7±0.2	67±7	10±4	0.10±0.04
15	7±1	19±6	7±2	0.8±0.2	65±8	9±3	0.11±0.04
20	6±1	23±3	7±2	0.5±0.2	63±5	9±3	0.07±0.02
25	6.4±0.6	24±1	8.3±0.9	0.6±0.1	60±2	7.2±0.8	0.07±0.01
30	7±2	22±3	7±2	0.5±0.1	62±6	9±3	0.07±0.02
40	6±2	20±3	6±3	0.4±0.2	67±7	11±6	0.07±0.03
50	5±1	22±4	7±3	0.4±0.1	65±7	9±4	0.06±0.03
60	6±2	22±4	7±3	0.3±0.2	65±8	9±4	0.04±0.02

* Indicative values, as C cannot be accurately quantified by EDS

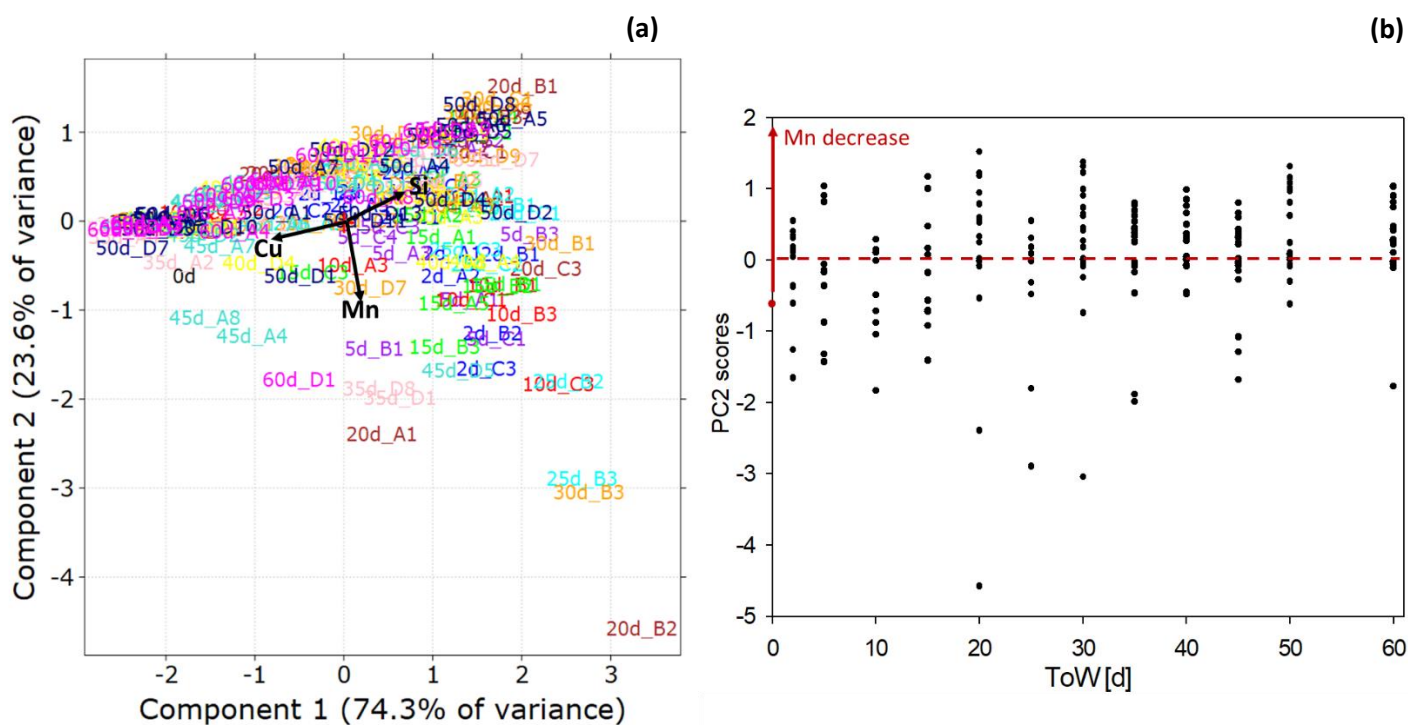


Figure S2: (a) Loading and Score plot for the first (PC1, explained variance 74.3%) and the second (PC2, explained variance 23.6%) component of the PCA model related to the EDS analyses of dark spots on the surface as a function of ToW. Variables included in the calculation are the amount of Cu, Mn and Si. Objects, corresponding to the spots analysed, are labelled with the related days of ToW. (b) PC2 Scores plotted as a function of ToW of the related objects. The score value corresponding to the interdendritic eutectic microconstituents before ageing (EDS data in Table 1 in the main text) is reported at ToW=0 days.

Figure S2 is related to the PCA model for the EDS analyses of dark spots on the surface as a function of ToW. The second principal component (PC2) is mainly related to the Mn amount (PC2 negative loading) and PC2 scores plotted as a function of ToW (Figure S2b) show that Mn amount in the spots tends to progressively decrease with time.

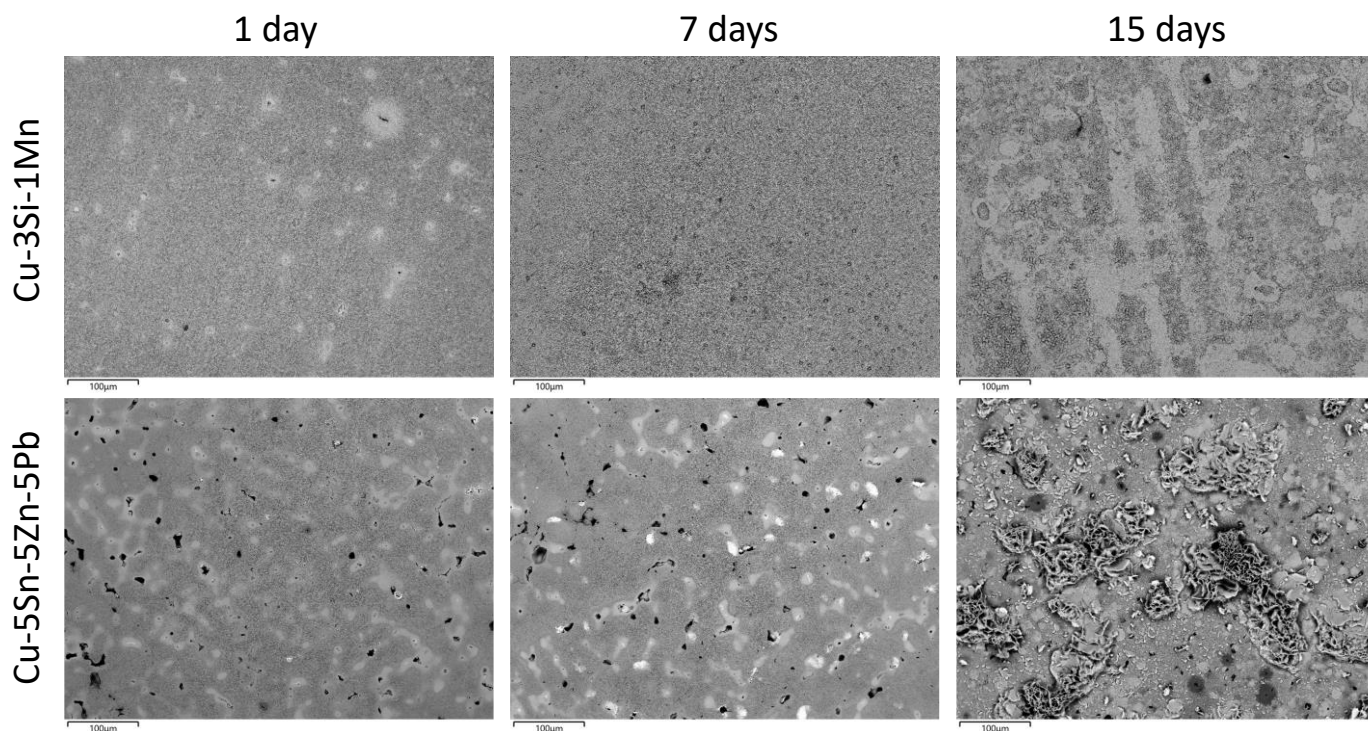


Figure S3: SEM-BSE images of Cu-3Si-1Mn and Cu-5Sn-5Zn-5Pb after immersions of 1, 7 and 15 days in artificial acid rain.

Figure S3 shows the morphology of the patinas formed on Cu-3Si-1Mn and Cu-5Sn-5Zn-5Pb surface during immersions of 1, 7 and 15 days in artificial acid rain and investigated by SEM-BSE observations. The presence of a surface film is clearly detected despite the low image magnification and is confirmed by SEM-EDS analyses carried out on large areas ($1.0 \times 0.5 \text{ mm}^2$) at 10 kV acceleration voltage (Tables S1 and S2). On Cu-3Si-1Mn the surface film is more homogeneous than on Cu-5Sn-5Zn-5Pb. Table S1 shows that its O content is almost constant during the immersion (about 10 wt%), while it results progressively depleted in Si (from 3.5 wt% in the alloy, to 0.2 wt% after 15 days) and enriched in C (up to 6.3 wt% after 15 days of immersion). Mn resulted selectively corroded because its content decreased from 0.8 in the alloy to 0.1 wt% after 1 day immersion, then increased to 0.4 wt% after 15 days of immersion. A minimal Cl contamination and no S are detected.

Table S1: SEM-EDS analyses (expressed in wt%) carried out on of Cu-3Si-1Mn after immersions of 1, 7 and 15 days in artificial acid rain (SD = standard deviation).

<i>Cu-3Si-1Mn</i> (wt%)	<i>C*</i>	<i>O</i>	<i>Si</i>	<i>Cl</i>	<i>Mn</i>	<i>Cu</i>	<i>Si/Cu</i>
Bulk	-	-	3.5	-	0.8	95.6	0.0366
SD	-	-	0.2	-	0.2	0.5	
1 day	2.8	10.1	0.8	0.1	0.1	86.2	0.0093
SD	0.7	0.2	0.2	0.1	0.1	0.9	
7 days	6.4	9.9	0.3	0.1	0.2	83.0	0.0036
SD	0.3	0.1	0.0	0.0	0.3	0.5	
15 days	6.3	10.1	0.2	0.1	0.4	82.9	0.0024
SD	0.2	0.3	0.1	0.1	0.1	0.3	

* Indicative values, as C cannot be accurately quantified by EDS

Table S2: SEM-EDS analyses carried out on of Cu-5Sn-5Zn-5Pb after immersions of 1, 7 and 15 days in artificial acid rain (SD = standard deviation).

<i>Cu-5Sn-5Zn-5Pb</i> (wt%)	<i>C*</i>	<i>O</i>	<i>Cl</i>	<i>Ni</i>	<i>Cu</i>	<i>Zn</i>	<i>Sn</i>	<i>Sb</i>	<i>Pb</i>	<i>Cu/Zn</i>	<i>Cu/Sn</i>	<i>Cu/Pb</i>
Bulk	-	-	-	1.1	85.0	4.6	5.1	0.6	3.7	18.6	16.6	23.1
SD	-	-	-	0.5	0.6	0.1	0.2	0.1	0.3			
1 day	4.7	6.7	0.1	0.8	76.4	2.3	5.6	0.5	3.0	33.8	13.7	25.9
SD	0.1	0.4	0.1	0.9	1.2	0.2	0.4	0.2	0.2			
7 days	6.8	7.5	0.0	0.5	73.0	1.8	5.4	0.5	4.5	39.9	13.5	16.3
SD	0.3	0.3	0.0	0.4	0.8	0.2	0.2	0.1	0.3			
15 days	8.0	9.6	0.0	0.3	28.6	0.8	2.7	0.2	49.7	36.7	10.7	0.6
SD	0.2	0.3	0.0	0.5	5.3	0.2	0.3	0.1	5.4			

* Indicative values, as C cannot be accurately quantified by EDS

On Cu-5Sn-5Zn-5Pb, as expected, selective dissolution of Zn occurs, as it drops from 4.6 wt% in the alloy to 0.8 wt% in the patina after 15 days of immersion. Meanwhile, C and O enrichments are detected, with contents going respectively from 4.7 to 8.0 wt% and from 6.7 to 9.6 wt%, at immersion times from 1 to 15 days. The surface Sn content changes from 5.1 wt% in the alloy to 2.7 wt% after 15 days. However, due to the marked concomitant decrease in Cu, the Cu/Sn ratio significantly decreases from 16.6 in the alloy to 10.7 after 15 days of immersion, suggesting a continuous relative surface enrichment in Sn (as tin oxide/hydroxide), due to the low solubility of tin corrosion products. Pb undergoes an initial selective dissolution, as indicated by a decrease in its content from 3.7 wt% in the alloy to 3.0 wt% after 1 day, but at the end of the immersion Pb concentration reaches 49.7 wt% and the Cu/Pb decreases from 23.1 to 0.6.

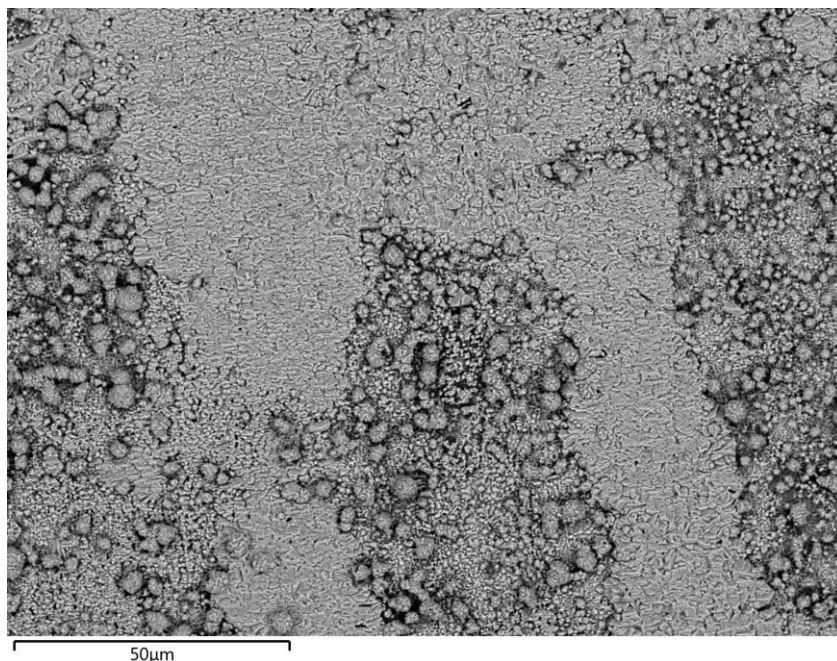


Figure S4: SEM-BSE images of Cu-3Si-1Mn bronze after 15 days of immersion in artificial acid rain.

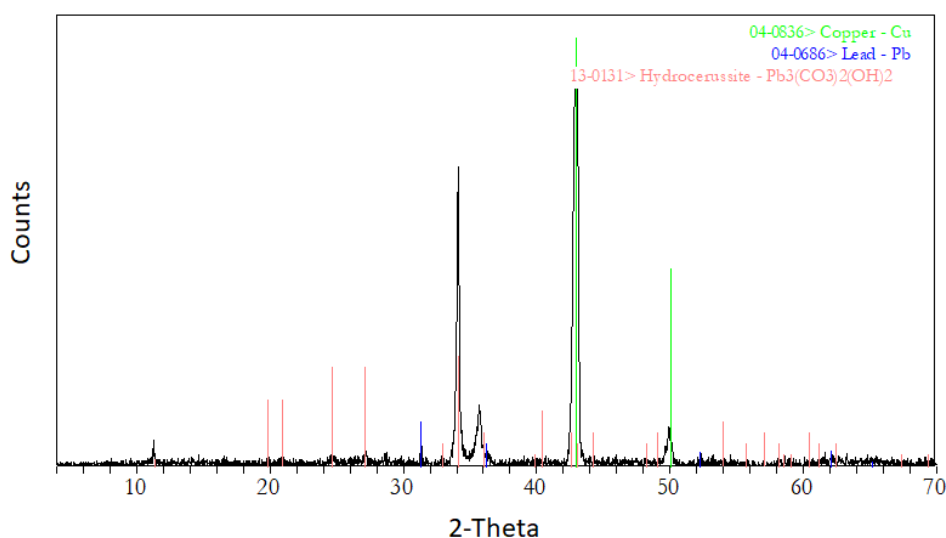


Figure S5: X-ray diffraction (XRD) patterns of patina formed on Cu-5Sn-5Zn-5Pb quaternary bronze surface after 15 days of immersion in artificial acid rain.

XRD surface analyses, carried out with a Bruker D8 Advances diffractometer (Bruker, Billerica USA) equipped with Cu tube, in the 2θ range of 4-70 degree, revealed that Pb rich precipitates, characterised by a rosette morphology, consisted of hydrocerussite (Figure S3).